Delft University of Technology
Master of Science Thesis in Computer Engineering

# UWB based wheelchair pose tracking

**Markus Jacobus Adrianus Jozefus Schrauwen**


TU Delft Delft University of Technology

# UWB based wheelchair pose tracking

Master of Science Thesis in Computer Engineering

Embedded and Networked Systems Group
Faculty of Electrical Engineering, Mathematics and Computer Science
Delft University of Technology
Mekelweg 4, 2628 CD Delft, The Netherlands

Markus Jacobus Adrianus Jozefus Schrauwen
mschrauwen@student.tudelft.nl
markschrauwen@gmail.com

14-03-2021

**Author**
Markus Jacobus Adrianus Jozefus Schrauwen (mschrauwen@student.tudelft.nl)
(markschrauwen@gmail.com)
**Title**
UWB based wheelchair pose tracking
**MSc Presentation Date**
22-03-2021

**Graduation Committee**

| | |
|---|---|
| dr. ir. Marco Antonio Zúñiga Zamalloa (chairman) | Delft University of Technology |
| dr. ir. Gerard J.M. Jansen | Delft University of Technology |
| dr. Rienk Michiel Arjen van der Slikke | The Hague University Of Applied Sciences, Delft University of Technology |

**Abstract**

Many wheelchair users actively engage in wheelchair sports, for instance in the Paralympics. Trainers increasingly use the developments in sports technology for analysis. But wheelchair athletes do not benefit as much from these developments. A wheelchair can, for instance, disturb signal transmission. Recently, a set of studies describe the development of a wheelchair measurement system, the *Wheelchair Mobility Performance Monitor* (WMPM). It monitors wheelchair kinematics based on a wheelchair model and two *Inertial Measurement Unit*s (IMUs). The WMPM also gives *relative* location and orientation i.e. relative pose. But this does not allow for game analysis, which requires the *absolute* location of an athlete. A way to obtain the absolute location of an athlete is the use of *Ultra-wideband* (UWB) technology. It is often used due to its relatively high ranging accuracy and affordability. However, UWB signal transmission can be disturbed due to *Non-Line-Of-Sight* (NLoS) situations, where the body of an athlete, or the wheelchair, is located between two UWB nodes. This reduces the localization precision and accuracy. Game dynamics, i.e. quick changes in direction and velocity, also reduce the UWB localization precision and accuracy. Separately, UWB and the WMPM are not sufficient for proper absolute pose tracking. But a combination of these systems, i.e. sensor fusion, could be a good alternative. To provide trainers with real-time tracking data, the sensor data of these systems need to be fused on an embedded system. This requires an efficient UWB localization solution. A recent algorithm by Larsson formulates a localization problem with an easier-to-compute linear eigenvalue approach. In this work, this approach is validated and compared with a previous implementation via simulations and measurements. We show a execution time that is 5 times faster, without accuracy loss. An *Unscented Kalman Filter* (UKF) is implemented to fuse WMPM and UWB data and it is improved with a Rauch-Tung-Striebel smoother. An IR-camera system (Optitrack), providing the ground truth, is used to validate the UKF. The solution has a *Root Mean Square Error* (RMSE) of less than 20 cm in dynamic wheelchair situations. This work provides a basis for further development of a platform where WMPM and UWB are integrated for paralympic sports.

*"Now, this is not the end. It is not even the beginning of the end. but it is, perhaps, the end of the beginning."* – WINSTON CHURCHILL

# Preface

There has been a trend of measuring and registering physical health-related parameters of oneself. This trend was coined in 2007 by Gary Wolf and Kevin Kelly as the 'Quantified Self' [1, 2]. However, coaches of sports teams were already tracking the behavior and performance of their athletes [23] in the 1970s [35]. There are many reasons for coaches to track these parameters, to name a few: evaluation, diagnosis, and prediction. This work tries to make a small contribution in the area of sports wheelchair tracking.

A lot of people have helped me to get to this point. I am taking the opportunity to briefly address some of them.

Thanks to the Hague University (THUAS) for granting me the opportunity to do this part-time master. Thanks to Carlijn and Daniel for providing access to the 'Bewegingslab' and for their help in setting up the Optitrack system.

Thank you Marco (Zuniga), you were my supervisor for over a year and the one who introduced UWB to me. Your enthusiasm and your questions that often probe the greater structure of my project were helpful and inspirational.

Thanks to Rienk van der Slikke. You have been a dear colleague (and my boss) and you provided the theme of this project for which I am grateful. Thank you, for your quick responses, your advice, and the help you gave me during the WMPM measurements.

Thanks to Vinay. You have answered my questions about your master thesis a couple of times and that was really helpfull.

A special thanks to Herre Faber. Not only have you been my colleague in my time at THUAS, but in those years you also became one of my closest friends. The short time we worked on a part of the localization section of this project has been one of the most enjoyable aspects. Your ability to effortlessly find my mistakes with pinpoint accuracy, has helped a lot during the years (and admittingly gave a lot of frustration).

Birgit, my best friend, my wife, the mother of my children, my love. You know my 'need to stay active' like no other and have helped to restrict, stimulate and facilitate it. I do not know, how I could have done this without you. Thank you.

Babette, you are the perfect distraction after a hard day of work. I am curious to see how you will grow up, and I hope you never stop growing.

A big thanks to everyone who helped me proofread this document, you were not always treated kindly.

Markus Jacobus Adrianus Jozefus Schrauwen

Delft, The Netherlands, 15th March 2021

# Contents

# Chapter 1

# Introduction

The sports industry is developing rapidly. Trainers and athletes frequently apply new technologies that provide information about the kinematics and performance of athletes [5]. This is also true for Paralympic sports [44, 34, 45, 49]. Some Paralympic sports involve the use of a wheelchair e.g. in basketball, fencing, rugby, and tennis. Analyzing the performance of wheelchair athletes is more challenging than in standard sports because wheelchairs can add significant interference and noise. For instance, in the case of *Ultra-wideband* (UWB), in *Non-Line-Of-Sight* (NLoS) situations.

## 1.1 Motivation

Performance monitoring of athletes is in a large part done by monitoring their absolute location and orientation during a match. This is called 'real-time absolute pose tracking' or in short pose tracking. Pose tracking of all athletes during a match allows for insightful game analysis. This project aims at improving pose tracking for wheelchair athletes.

### 1.1.1 Wheelchair monitoring

In a set of recent studies [47, 48, 50, 46], the development and improvement of the *Wheelchair Mobility Performance Monitor* (WMPM) is covered. It provides a wheelchair user with insights in wheelchair kinematics e.g. velocity, trajectory length, number of turns, etc. The WMPM consists of a mathematical model that uses specific wheelchair parameters and the data of two *Inertial Measurement Unit*s (IMUs). But it has a couple of shortcomings related to the fact that it is based on odometry[1]:

- Wheel skidding [48]. Here, a wheel of a wheelchair is slipping with the wheelchair barely moving because of the wheelchair inertia and the dynamic wheel friction.
- Wheelchair falls. Falls do not occur very often, but are nonetheless possible and will interfere with the WMPM output.
- Wheelchair jumps. Wheelchair collisions regularly occur during a match. Depending on the collision intensity, this could be interpreted as a jump. The point of impact is then a point of momentary rotation due to the wheelchair momentum.

The WMPM can also output relative pose as seen in figure 1.1, by using the starting pose of a wheelchair as a reference. However, this does not allow for game analysis as every user will have a different starting position. Furthermore, this relative pose

[1] A form of dead-reckoning.

tends to diverge. For example, a 'clean' wheel slip will not change the location of a wheelchair, but it will be registered as a movement by the IMUs. This will inevitably give an increasing error in the relative pose during a game. Additionally, wheelchair impacts could also displace the IMUs during a match. The increasing relative pose error can be reduced by incorporating technology that gives the absolute localization of an athlete.

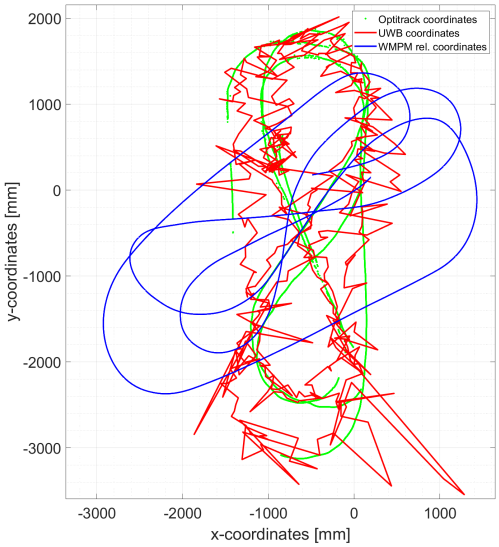


**Figure 1.1:** An example of a wheelchair measurement, obtained in this project, where the location of the wheelchair is tracked. It shows the output of three systems: the ground truth (Optitrack), UWB and the WMPM. The WMPM does not align with the ground truth.

### 1.1.2 UWB localization

Camera systems, e.g. *Marker Based Motion Capture System* (MOCAP), are often used in the localization of athletes. A MOCAP system has a localization accuracy in the submillimeter range. This allows them to be used as a ground truth system. But those systems have their disadvantages:

- they take a relatively long time to set up
- an athlete has to wear a MOCAP suit
- they are expensive (more than 20.000 €.)
- they give large amounts of data, which makes game analysis slower

There are several alternative indoor localization technologies [28, 41]. To name a few: Wi-Fi, Bluetooth and UWB. Of those technologies, UWB has the highest ranging accuracy. Ranging is the process of determining the distance between two (UWB) nodes, which is required for localization. The relatively high UWB ranging accuracy and the development of the *DecaWave D1000 Radio Chip* (DWM1000) have made UWB a popular research area. To illustrate this, over 250 paper have been written about UWB localization [3] since 2016.

#### 1.1.2.1 UWB localization accuracy

A localization accuracy of approximately 30 cm is reported in research that applies UWB in 'standard' sports [21, 9]. With an UWB node attached to the head of an athlete, an improved accuracy is reported of approximately 20 cm [33]. However, attaching an UWB node to the head of an athlete is not desirable as the movement

of the head of the athlete must be taken into account and because. It also potentially interferes with the performance of the athlete as the *Tag* (TAG) has some weight and can be displaced in dynamic situations.

Furthermore, UWB localization data has a significant amount of disturbance as can be seen in figure 1.1. Simple filtering of this UWB data, for instance with a moving average or a Savitsky-Golay filter will improve the precision. But these filters will not compensate for the big jumps in UWB location which, for instance, could place a wheelchair athlete outside the court. In general UWB is relatively accurate but lacks precision (which is the other way around with the WMPM).

#### 1.1.2.2 UWB wheelchair application

In the ideal situation, a wheelchair athlete should not notice any device attached to his/her body (e.g. the head). An obtrusive system could otherwise potentially distract an athlete from the game. This can be prevented, for instance, by attaching a device (e.g. an UWB node) to the backseat or frame of the wheelchair.

But this type of UWB node attachment, introduces NLoS. Here the wheelchair and the athlete disturb or block the UWB signal transmission or reception, which negatively influences the ranging accuracy. Another factor that reduces the UWB ranging accuracy in sports, is game dynamics [10]. Wheelchair sports are known for their dynamics: the quick changes in direction and velocities.

### 1.1.3 Goal

There is no easy-to-use and affordable wheelchair localization system that provides real-time pose tracking of wheelchair athletes. UWB could be a good addition to the WMPM, alleviating these problems. It is unclear if this will give an acceptable localization precision of 20 cm or less in a dynamic setting. Next to that, the solution should be as unobtrusive as possible and localization should be as fast as possible to deal with game dynamics.

The goal of this project is:

To improve the existing WMPM system with UWB in such a way that it allows for real-time wheelchair pose tracking.

## 1.2 Contributions

The key contributions that this work provides are:

1. An overview of recent UWB research related to localization.
2. An overview of recent progress with relation to sports localization.
3. A state-of-the-art analysis and implementation of an improved localization algorithm.
4. A sensor fusion implementation and evaluation of UWB and the WMPM.

## 1.3 Thesis organization

First, a global overview related to this project will be given in chapter 2 with a section about relevant research. Followed by the description of the work done concerning localization in chapter 3. This is followed by chapter 4 which covers the combination of WMPM with UWB data. The measurement setup is covered in chapter 5 and followed by the evaluation in chapter 6. Finally, chapter 7 describes the conclusions and future work.

# Chapter 2

# Background & Related work

This chapter gives UWB background information and an overview of related work. UWB is briefly introduced in section 2.1 and followed by section 2.2 that explains ranging and localization. Section 2.3 gives an overview of recent research about (wheelchair) sports and UWB.

## 2.1 UWB

UWB is a radiofrequency technology that allows for data transmission between two or more UWB devices [26]. Besides a 'wide bandwidth' (500 MHz) another typical property of UWB is the power spectral density limitation of −41.3 dBm/MHz. This results in a couple of improvements compared to other radio technologies [11]:

- immunity to multipath fading
- interference mitigation
- increased throughput
- higher timing resolution

The high bandwidth allows for 'sharp' pulses in the time-domain which gives an improved timing resolution. This is important for the quality of distance estimation and in extend for localization. Of the existing radiofrequency technologies UWB *IEEE Ultra Wide band* (IEEE 802.15.4) has the highest localization accuracy [41]. Because UWB has little interference with existing (narrow-band) radio systems, it is ideal for integration in existing systems.

## 2.2 Ranging and localization

Ranging is the process of measuring the distance between two UWB nodes. A stationary UWB node, with a known location, is called an *Anchor* (ANC). A moving UWB node is called a TAG and has an unknown location. If the distances between a TAG and at least three other ANCs are measured, a unique location of the TAG can be calculated. This is called *true-range multilateration*.

### 2.2.1 Accuracy

The localization accuracy depends on the ranging accuracy. The theoretical UWB accuracy can be estimated with the radar range resolution $\delta_r$ [22, 37].

It is approximated by $\delta_r \approx \frac{c}{2B}$ where $B$ is the bandwidth of the UWB pulse. This is shown in figure 2.1 and illustrates a theoretical ranging accuracy of approximately 5 cm at 3.1 GHz (the lower bound of the UWB frequency range). Most papers, report

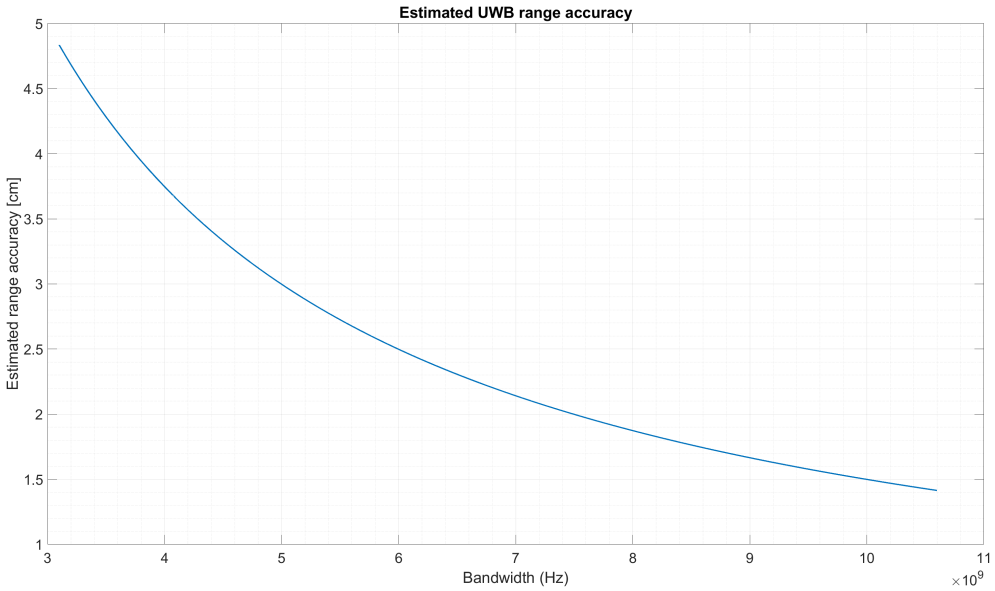


**Figure 2.1:** The ranging accuracy of UWB related to the bandwidth with the assumption of *Line-Of-Sight* (LoS).

a lower localization accuracy. Also companies with a focus on UWB report a lower localization accuracy as shown in section B.7. This mismatch can be explained by some limitations of UWB technology:

- timing inaccuracies.
- measurement disturbances e.g. NLoS.
- signal reflections.
- absorption by the human body [27, 28]

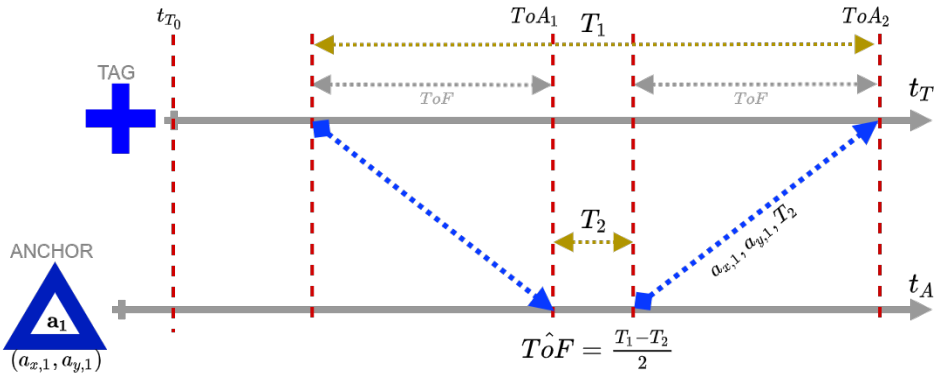


**Figure 2.2:** A schematic example of *Two Way Ranging* (TWR). The x-axis represents time. Please note that this figure only shows one ranging example. At least three unique ranges are necessary to localize the TAG.

### 2.2.2 Time of Arrival

In order to measure the distance ($d$) between an ANC and TAG the duration or *Time-of-Flight* (ToF) has to be known, as shown in figure 2.2. The distance can be calculated by: $d = ToF \cdot c$, where $c$ is the speed of light. Measuring the ToF requires that the TAG and ANC are synchronized, i.e. have the same absolute time reference. When a TAG and ANC are synchronized, their distance can be estimated by the

*Time-of-Arrival* (ToA) of a message. This is, for instance, done with TWR as seen in figure 2.2. Here ranging is achieved by sending two messages between two UWB nodes. Then, the average ToF is calculated and used to estimate the distance.

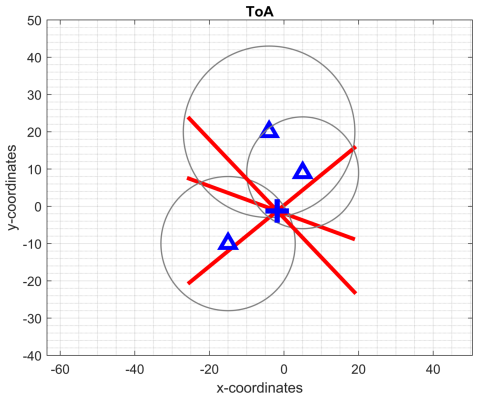


**Figure 2.3:** Example of simple ToA localization in the noiseless case. The blue cross illustrates the location of the TAG. The blue triangles visualize the ANCs. This is further explanation in the text.

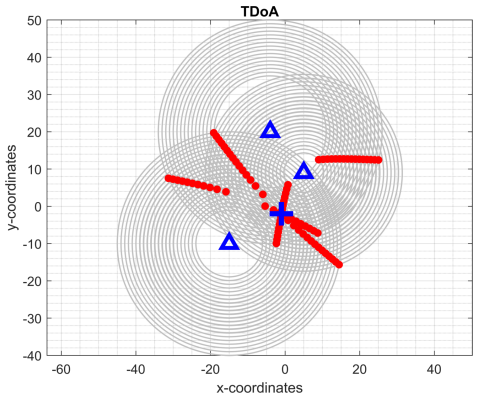


**Figure 2.4:** Example of simple *Time Difference of Arrival* (TDoA) localization without noise. The blue cross illustrates the location of the TAG. The blue triangles visualize the ANCs. This is further explanation in the text.

Figure 2.3 illustrates simple localization of a TAG, with TWR, in the noiseless case. Each range between a TAG-ANC pair can be expressed as a circle. This gives a set of intersecting circles. A line can be drawn on each circle intersection pair, this is called an emitter line. The intersection of emitter lines represents the location of the TAG. In practical ranging, there is always an amount of disturbance (or noise). Localizing a TAG in those situations requires a more elaborate kind of localization (see chapter 3).

### 2.2.3 Time Difference of Arrival

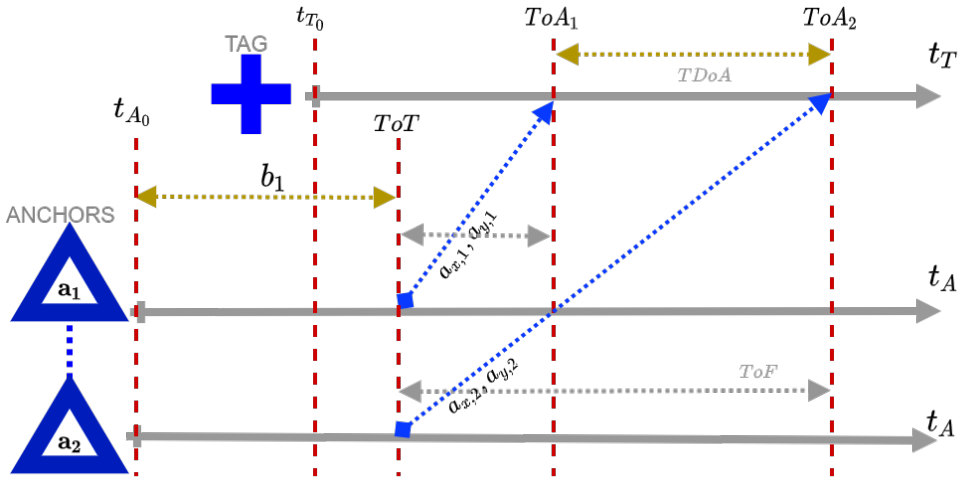


**Figure 2.5:** A schematic example of TDoA. The x-axis represents time. The ANCs are synchronized, i.e. have the same temporal reference. At least 4 ANCs are needed to uniquely localize a TAG.

Maintaining synchronization between a TAG and ANCs comes with disadvantages. For instance, TWR is generally slower than other techniques. Sending multiple messages between a TAG and ANC will take time. A way to evade the synchronization of a TAG and ANC, is applying TDoA or *pseudorange multilateration*.

In TDoA, the ANCs are synchronized, but not with the TAG. This method uses the ToA *difference* of each unique TAG-ANC pair. With the ToA differences the unknown temporal offset $b1$ can be estimated as shown in figure 2.5. Please note that in this case the ToA can be measured, but not the ToF. TDoA requires accurate synchronization between the ANCs. To achieve accurate synchronization, *Global Positioning System* (GPS) satellites for instance, use atomic clocks. In an UWB setting, synchronization of the ANCs often occurs via cables or with dedicated wireless transceivers. To illustrate the importance of accurate synchronization we give the following example. Suppose that a UWB system has a synchronization error $\tau_{err}$ of 1 ns, this gives a distance error $d_{err} = 1\,\text{ns} \cdot 299\,792\,458\,\text{m}\,\text{s}^{-1} \approx 30\,\text{cm}$.

Simple localization with TDoA is shown in figure 2.4. The 'difference' in *Time Difference of Arrival* can occur at many possible circle-pairs. For instance, a TDoA of 5 ns could be based on the ToAs 13 ns-8 ns but also the ToAs 16 ns-11 ns. This explains the need to draw multiple circles per TAG-ANC pair. The intersection of each possible circle is visualized with a red dot, the emitter dots[1]. Similarly to the ToA example, the intersections of the emitter dots, which have a hyperbolic trend, indicate the location of the TAG.

### 2.2.4 Wheelchair sports

In regular sports, an athlete is not limited in the way the athlete can move (this excludes specific game related sport rules, e.g. in boxing one can not use their elbows). But not everyone has access to 'regular' motion. The Paralympic Sport Committee recognizes eight types of physical disability and one of them is *loss of limb, or limb deficiency*. An athlete, in this Paralympic Sports category, is bound to a wheelchair.

There are several wheelchair sports: wheelchair tennis, wheelchair basketball, wheelchair curling, etc. Each wheelchair sport can have a specific optimal wheelchair configuration and even individual wheelchair modifications are possible for maximum performance. Figure 2.6 shows a typical sports wheelchair. Some examples of specific wheelchair parameters are: height of the seat, wheelchair mass, grip of the rim of the wheel [8, 51]. The optimal wheelchair, most likely has a minimal design. This reduces the options to mount an UWB TAG to the wheelchair as covered in chapter 5.

Depending on the game, also a different number of athletes are allowed on the court. For instance, in wheelchair tennis, this is two or four. An example of wheelchair rugby is shown in figure 2.7, this sport allows ten athletes on the court. The maximum number of athletes that have to be simultaneously tracked, with a wheelchair pose tracking solution, is ten.

## 2.3 Related work

This section gives an overview of research related to localization in sports, localization in wheelchair sports and recent UWB research.

[1] Choosing an appropriate resolution will allow for drawing an *emitter line* which is not done in this case to improve the clarity.


**Figure 2.6:** A typical sport wheelchair, Celeritas 300.

**Figure 2.7:** Example of wheelchair sports (photo by Frank van Hollebeke).

### 2.3.1 Localization in sports

Leser et. al. 2011 [18] gives an overview of localization technologies and their implications related to sports. They use the in Lee et. al [17] coined definition of *intelligent space* (IS) to describe rooms equipped with sensors that can localize athletes. It illustrates the idea of how an unobtrusive setup could be designed for game sports to assist trainers in their activities. An IS could, for example, give feedback regarding: tactics, fatigue, and the substitution of players. They state that it is crucial for a localization system to have an accuracy between 15 cm and 20 cm in dynamic conditions. Additionally, the update rate should at least be between 10 Hz-15 Hz. These conclusions, give a lower-bound for the accuracy and update rate for this project.

The accuracy of UWB is investigated in Leser et. al. 2014 [19] concerning 'time-motion analysis'. Time-motion analysis, covers the time spent on a movement during a game. In a set of measurements, the TAG was placed on the head of an athlete because that gave the best accuracy. 13 athletes got a trundle[2] to measure the covered distance. The UWB traject length, compared to the trundle distance, gave an average difference of 3.45 % $\pm$ 1.99 %. Leser et. al. conclude that UWB provides sufficient accuracy for time-motion analysis in basketball. However, this work does not say that UWB is usable for game analysis or pose tracking.

Sports activities are generally characterized by fast changes in direction and velocity, i.e. the dynamics. Ridolfi et. al. 2018 [33] paints a better picture about the game analysis potential of the UWB. They assess UWB, the localization of an athlete, in a set of dynamic situations for 'regular' sports. First, they investigate the effect of on-body TAG and secondly implement two different localization filters. The influence of TAG placement on the human body was done by considering three metrics: accuracy, packet loss and the number of visible anchors (i.e. LoS) [3]. The different investigated TAG placements are visualized in figure 2.8. They concluded that the best TAG

[2] A trundle is a stick with a wheel on the end of it, touching the ground that, while moving, tracks the covered distance.

[3] Packet loss occurs when a packet or frame fails to reach a destination (intact). Packet loss is influenced by shadowing and small-scale fading. **Small-scale fading** refers to the fast changes of the phase and amplitude of a signal over a short period of time or a short distance. It is also called Rayleigh fading. **Shadowing** refers to the effect that something close to a source (ANC) will cast a 'shadow' and in effect block the path between ANC and TAG.

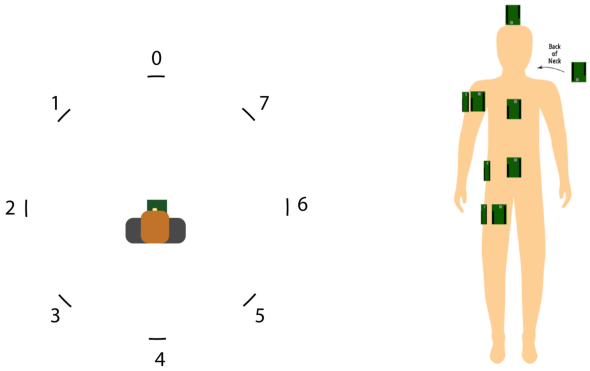


**Figure 2.8:** Setup of TAG and ANC placement w.r.t. the human body. Not shown in the figure are the postures and dynamic movements. By Ridolfi et. al. [33].

placement, concerning packet loss, is the head of an athlete, similar to Leser et. al. [19]. However, as stated in section 1.1.2.1 this is not ideal because attaching the TAG to the head potentially interferes with the performance of the athlete.

Ridolfi et. al. furthermore looked at the improvement of athlete localization with the *Extended Kalman Filter* (EKF) and the *Particle Filter* (PF). The disadvantage of a PF is the increased computational power that is required, but it can handle non-linearities better than the EKF, which are always present in dynamic sports situations. Bias compensation, NLoS detection and path determination improved the performance of these filters with 30 %. They finally conclude that the best localization filter depends on the type of activity, but they do not give any guidelines.

In a football environment, Martinelli et. al. 2019 [21] tested the performance of a custom UWB system. The objective was to measure the influence of the ANC placement at 1 m, 1.6 m and 2 m height. This influence was researched with three metrics: accuracy of location, packet loss and packet loss concerning the ANCs. The average height of a football player (1.6 m) gave the best results with an *Root Mean Square Error* (RMSE) of 31 cm and a package loss of 28 %. The conclusion seems obvious as this height, gives the shortest distance between an ANC and a TAG, which was mounted to the back of an athlete.

A recent review by Rico et. al. 2020 [32] looked at different tracking methods concerning tactical variables in team sports. They conclude from 72 articles that UWB technology is not used to date for tactical tracking and that UWB provides sufficient accuracy for tactical tracking in a sports setting. Additionally, they state that a system that is used in training and competition will facilitate the assessment of collective tactical behavior. There are, however, commercial localization systems like Kinexon [4] that are being used for tactical tracking. However, the quality of the game analysis information is unkown, moreover it is expensive for an UWB system.

The following list summarizes the most important findings in this subsection:

- The minimium UWB update rate suggested for a dynamic sports setting is between 10 Hz-15 Hz [18].
- The minimum localization accuracy should be 20 cm or less in a dynamic sports setting.
- The placement of an UWB TAG on the head of an athlete gives the best accuracy [33].

[4] https://kinexon.com/technology/tactical-analysis

- There is no research indicating the use of UWB for tactical purposes (i.e. game analysis) [32].

### 2.3.2 Wheelchair research

Slikke et. al. 2015 [47] developed a wheelchair kinematics measurement system based on a three IMU configuration, the first version of the WMPM. Each wheel had one IMU and another IMU was mounted to the base of the wheelchair. The system performed well, based on a comparison with the ground truth, except for moments of wheel skidding. The displacement and speed error were respectively $RMSE < 0.05\,\mathrm{m}$ and $RMSE \leq 0.01\,\mathrm{m\,s^{-1}}$ and averaged over 20 measurements. The results provide a setup that can be used for wheelchair kinematics analysis. However, the absolute location can not be tracked with an IMU based system. This is due to the requirement of an absolute reference, which an IMU does not have.

To determine the quality of UWB localization related to wheelchair sports Perrat et. al. 2015 [29] give a qualitative assessment. They looked at TAG placement, update rate, data gaps and localization in static- and dynamic situations. Their findings suggest that the TAG update rate (4 Hz, 8 Hz and 16 Hz), and the number of wheelchairs present on the court do not significantly affect the localization accuracy. An evaluation gave a localization error of 37 cm ($\sigma = \pm$ 24 cm) in a fake wheelchair rugby match, with one person in a wheelchair and multiple TAGs on the court. The covered distance, or traject length, was analyzed and compared to a ground truth reference which can be used as a basic test to evaluate the performance of a localization setup. The results show a traject length error of 0.5 % after applying a three-pass moving average filter. Furthermore, the presence of *data gaps* was analyzed, in a real match with eight wheelchair athletes. A data gap, was defined as an *outage of data* for more than 0.5 s. On average, every 14.0 s a data gap was observed. It is concluded, that a real match with eight players and a referee should not degrade the localization performance. However, their conclusions could be incomplete. When more athletes are present on the court there must be a higher probability of NLoS and the authors do not explain why the results do not show this. A reason for not observing a reduced localization accuracy, when more wheelchairs are on the court, could be that the ANCs are placed on a mount of approximately 4 m height. Placing an ANC on a high stand will prevent NLoS as seen in figure 2.9.

Slikke et. al. 2017 [50] compared an UWB localization system (ITS Ubisense) to the WMPM. To this end 'speed zones' concerning speed and distance were defined. The speed zones were used to compare the speed and distance measurements of the two systems. At speeds lower than $2.5\,\mathrm{m\,s^{-1}}$ minor differences between the systems were observed. A hybrid solution of the WMPM and a UWB was concluded to potentially serve a new 'golden standard' for measuring wheelchair kinematics.

To conclude, UWB has been previously used in wheelchair research, but the results are limited. It would, moreover, be advantageous to mount the ANCs on a high stand as shown in figure 2.9.

### 2.3.3 UWB research

This subsection gives an overview of recent research about UWB localization, moreover it supports the future work section in section 7.2.

ToA and TDoA are covered in section 2.2, but it does not say which one is more accurate, which could support the choice in the technology used in this work. In work by R. Kaune [15] the accuracy of ToA and TDoA is investigated and uses the well-known *Cramer Rao Lower Bound* (CRLB). The CRLB is a theoretical lower bound of the variance of an unbiased estimator. A lower CRLB would allow for more precise localization. The CRLB is shown to be identical for ToA and TDoA with

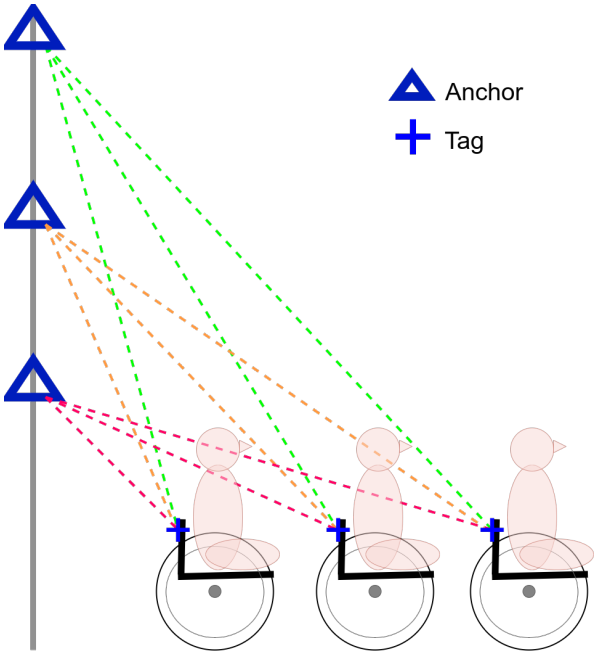


**Figure 2.9:** A diagram that relates the ANC height with NLoS in a wheelchair setup. The probability of NLoS gets lower as the ANCs are placed higher.

a fixed reference, and this is aligned with findings in Sathyan et. al. [38]. A set of Monte Carlo simulations furthermore showed that there are no differences in accuracy between ToA and TDoA. This suggests that the choice of using ToA or TDoA should not depend on the CRLB or the localization accuracy. However, simultaneously both Kaune and Sathyan [15, 38] note that the cost function of TDoA is more non-linear. Which explains why 'in practice' ToA tends to give a better localization accuracy.

In the last few years, different research groups showed new and exciting variations of UWB ToA and TDoA system. This subsection will give an overview of these state-of-the-art concepts.

The localization accuracy of an UWB setup could be in the millimeter range if several ANCs are used. But this is not practical. Having only one ANC would be optimal in terms of ease-of-setup and cost-effectiveness. GrossWindhager et. al. [12] developed such an UWB system, called SALMA, as seen in figure 2.10. By exploiting *multipath components* (MPC) it can work with a single ANC with an omnidirectional dipole antenna. This setup does not need calibration or training, it only needs a crude floorplan as seen in figure 2.10. A maximum update rate of 12.5 Hz is reported due to the computational load of this method. The system is tested in a room with people and they found an average error of 34 cm and the 90% error was below 79 cm. This work provides a means for future research and a future iteration could give a solution that makes a wheelchair UWB setup much simpler.

The number of TAGs in TWR is practically limited, see figure 2.11, due to the message overhead and message collision avoidance. TDoA reduces this problem, but it requires tight synchronization between the ANCs and the messaging is still sequential. GrossWindhager et. al [11] created a system called SnapLoc that reduces some of these limitations. In SnapLoc a TAG does not actively transmit messages, instead it predominantly receives ANC messages see figure 2.11. An *INIT* message is send by the TAG at the start. Each ANC responds after time $\Delta_R$ and an individual delay $\delta_i$ with a *RESP* message. This alleviates the need for tight clock synchronization

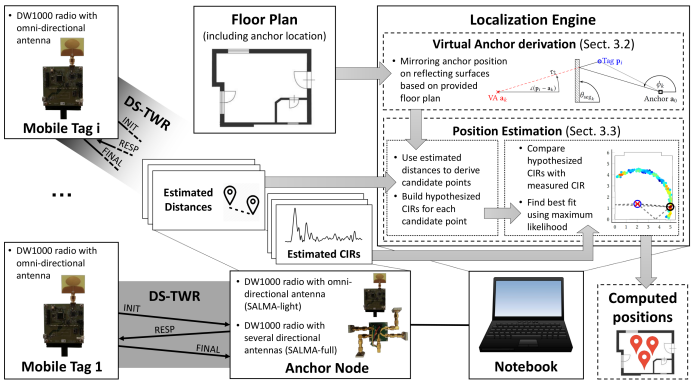


**Figure 2.10:** The overview of the SALMA system design. Courtesy of B. GrossWindhager [12].

between the ANCs. The system with the wired clock correction, compared to a wireless variant, gave the best results: with 90% error of 33.4 cm and a median error of 18.4 cm. A theoretical upper bound update rate is stated of 2.3 kHz.

Corbalan et. al. [7] created a system called *Chorus* that exploits UWB very similar to the work by GrossWindhager et. al. [11] with differences in implementation and methodology. This system only gives submeter accuracy due to a higher clock drift sensitivity and the TX inaccuracy [5]) of the DWM1000.

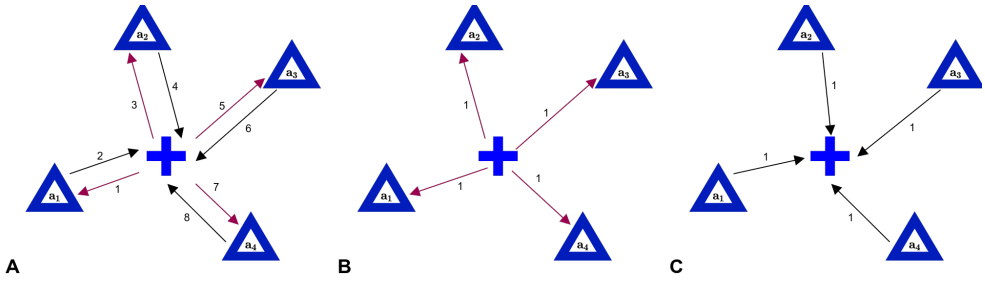


**Figure 2.11:** Different localization schemes, the blue sattelite represents an ANC. **A**: TWR. **B**: TDoA. **C**: The scheme applied in SnapLoc and Chorus.

Three main factors that negatively influence the localization accuracy are: hardware delay, clock drift and signal power. Sidorenkoab et. al. [39] describes a solution that improves the influence of clock drift and signal power. Clock drift is usually corrected via a *Phase Locked Loop* (PLL) but can be affected by signal power fluctuations. After warmup, three messages $(T_1, T_2, T_3)$ are send between two UWB nodes. When a clocks exhibits drift, then the timestamp differences $(\Delta T_{1,2}, \Delta T_{2,3})$ are different. Simple linear interpolation is used to correct this drift. There is however still a dependency on signal power due to the distance between the nodes. By sending three messages where the second message has a different signal strength, a relation is found between the measured signal strength and the timestamp error. The clock drift correction and signal power correction reportedly give a localization accuracy in the centimeter range. This work has a similar clock drift correction as described by Leugner et. al. [20]. These improvements could be implemented in a future version of this project to improve the ToA accuracy.

[5] Which has an accuracy of ≈ 8 ns which gives a maximum error of ≈ 2.4 m.

The update rate of an off-the-shelf Decawave UWB system is improved with a factor of 30 times ToA in Neuhold et. al. [25]. It operates by using 'beacons' and hardware interrupts for *timestamping* instead of embedding a TX timestamp to the header of the message. This allows for a reduction of the delay between receiving and transmitting and gives a higher precision. Because the HiPR system is more precise the ranging bias is more linear. This allows for more compensation of systematic errors.

#### 2.3.3.1 Conclusion

Perrat et al. [29] concluded that an update rate of 4 Hz-8 Hz-16 Hz does not significantly affect the localization when relative constant velocities are maintained. For this work, the best presumption is to use the highest attainable update rate.

Preliminary research was done by Slikke et. al. [50] concerning the use of UWB in wheelchair sports. They concluded that the combination of UWB and the WMPM could potentially serve as a new golden standard. This is aligned with the work of [29] and supports the motivation of this work.

Choosing an UWB based on ToA or TDoA accuracy is trivial as Kaune [15] showed that there is no theoretical accuracy difference. However, in practice ToA achieves better accuracy. This supports the choice for ToA in this project. Neuhold et. al. [25] described a way to achieve faster ToA. This is beneficial for the sensor fusion part of this project because a higher update rate will give more localization information.

# Chapter 3

# Localization algorithm

## 3.1 Introduction

Real-time localization should be as fast and accurate as possible. This section explains three main trilateration algorithms and their performance is evaluated in section 6.1. This first algorithm, is a previously used algorithm in a master thesis by the department of TU Delft Embedded and Networked Systems Group from Murphy [24]. The second algorithm is from the work of Larsson et. al. [16] that is based on an eigenvalue approach (section 3.3). Lastly, a recently devised algorithm by H. Faber is covered in section 3.4 in an attempt to improve Larsson. The covered trilateration methods are described for the 2D case and can be extended for the 3D case.

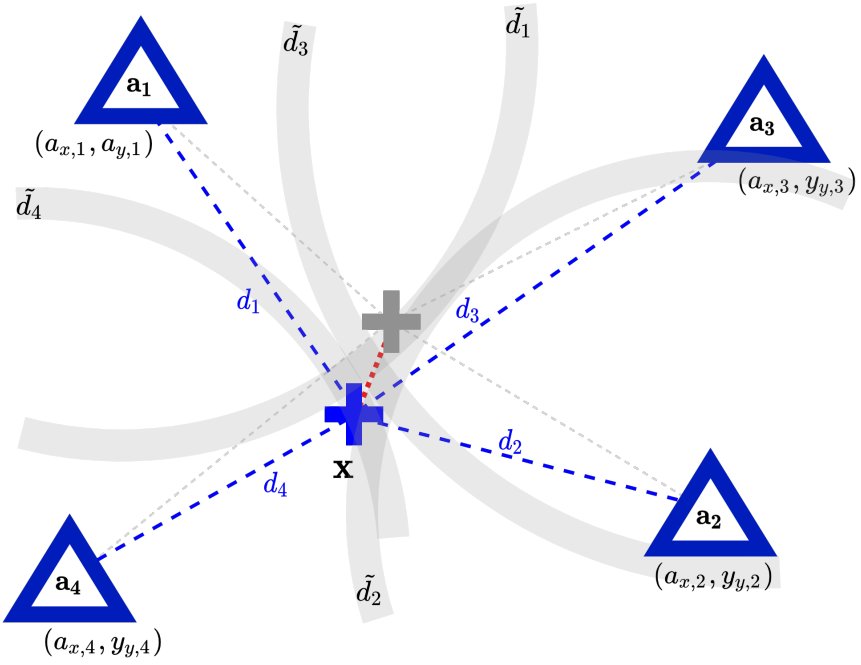


**Figure 3.1:** A schematic UWB setup. There are four ANCs illustrated by blue triangles. The gray cross designates the 'true' unknown location of the TAG. The blue cross illustrates the *estimated location* $\mathbf{x}$ of the TAG. A 'measured distance' between an ANC and a TAG is illustrated with a partial circle $\tilde{d}_j$.

Figure 3.1 shows a schematic UWB setup, with the definitions used in this section, that has $N$ anchors (in this case $N = 4$) and one TAG. Each ANC $\mathbf{a}_j$ ($j = 1..N$) has a known location $\mathbf{a}_j = [a_{x,j}, a_{y,j}]^T$ and is illustrated with a blue triangle. The 'true', but unkown TAG location is designated with a gray cross. All measured ranges $\tilde{d}_j$, i.e. ranges with an error, serve as an input for a localization algorithm. A localization algorithm estimates the optimal TAG location $\mathbf{x} = [x, y]^T$ given the measured ranges. The estimated location of the TAG has a range $d_j$ to an ANC. Please note that there can be a difference between the estimated ANC-TAG distances $d_j$ and the measured ranges $\tilde{d}_j$.

## 3.2 Murphy algorithm

Murphy compares in [24] a set of trilateration algorithms for the mining company TBCC. His final method is based on a nonlinear least-squares approach (NLS). The NLS determines the optimal estimated location of a TAG. It needs a first 'guess' of the location of the TAG. In his case, the linear least-squares method is used as a first guess. Then the NLS iteratively tries to improve the estimation of the TAG by calculating the derivative of the error function $F(x, y)$. The largest derivative indicates the direction of most improvement. This process repeats until the amount of change has reached a sufficiently small number.

The distances $\tilde{d}_j$ can be represented by a circle. This circle symbolizes all the possible locations of a TAG based on that range, and this can be written in the circle equation as:

$$||\mathbf{x} - \mathbf{a}_j|| = \sqrt{(x - a_{x,j})^2 + (y - a_{y,j})^2} = \tilde{d}_j \tag{3.1}$$

To minimize the errors, the difference between the $\tilde{d}_j$ and the *estimated* distance $d_j$ must be found. Squaring the difference for each TAG-ANC pair and summing the difference gives:

$$F(x, y) = \sum_{j=1}^{N} \left(\tilde{d}_j - d_j\right)^2 = \sum_{j=1}^{N} f_j\,(x, y)^2 \tag{3.2}$$

The Newton iteration method for minimization needs an initial guess or start from where it will minimize the errors. An acceptable choice is obtained from the linear approach in the next section.

### 3.2.1 Linearized trilateration

Starting with the circle equation:

$$(x - a_{x,j})^2 + (y - a_{y,j})^2 = \tilde{d}_j{}^2 \tag{3.3}$$

A seemingly arbitrary but advantageous addition and subtraction of a term $a_{x,k}$ and $a_{y,k}$ gives:

$$(x - a_{x,k} + a_{x,k} - a_{x,j})^2 + (y - a_{y,k} + a_{y,k} - a_{y,j})^2 = \tilde{d}_j{}^2 \tag{3.4}$$

By expanding the terms in equation 3.4 and regrouping them one can get:

$$(x - a_{x,k})(a_{x,j} - a_{x,k}) + (y - a_{y,k})(a_{y,j} - a_{y,k}) = \tag{3.5}$$

$$\frac{1}{2}\left[(x - a_{x,k})^2 + (y - a_{y,k})^2 - \tilde{d}_j{}^2 + (a_{x,j} - a_{x,k})^2 + (a_{y,j} - a_{y,k})^2\right] = \tag{3.6}$$

$$\frac{1}{2}\left[\tilde{d}_k^2 - \tilde{d}_j{}^2 + d_{j,k}^2\right] = b_{j,k} \tag{3.7}$$

The term $b_{j,k}$ consists of three known terms, the distance $d_{j,k}$ between $ANC_j$ and $ANC_k$, the measured $ANC_j$-TAG distance $\tilde{d_j}$, and the measured $ANC_k$-TAG distance $\tilde{d_k}$. Then, choosing an arbitrary ANC $k$, for instance $k = 1$, allows for equation 3.5 and equation 3.7 to be written as:

$$\begin{bmatrix} (x - a_{1,x})(a_{2,x} - a_{1,x}) + (y - a_{1,y})(a_{2,y} - a_{1,y}) = b_{2,1} \\ (x - a_{1,x})(a_{3,x} - a_{1,x}) + (y - a_{1,y})(a_{3,y} - a_{1,y}) = b_{3,1} \\ \vdots \\ (x - a_{1,x})(a_{N,x} - a_{1,x}) + (y - a_{1,y})(a_{N,y} - a_{1,y}) = b_{N,1} \end{bmatrix}$$

Which can be written in matrix form:

$$\mathbf{Ax} = \mathbf{b} \tag{3.8}$$

This gives an initial guess of the location of a TAG which is used as input for non-linear least-squares optimization, explained in the next subsection.

### 3.2.2 Non-linear Least-squares optimization

To minimize the cost-function equation 3.2 it can be differentiated with respects to $x$ and $y$:

$$\frac{\partial F}{\partial x} = 2\sum_{j=1}^{N} f_j \frac{\partial f_j}{\partial x}, \qquad \frac{\partial F}{\partial y} = 2\sum_{j=1}^{N} f_j \frac{\partial f_j}{\partial y}$$

All TAG-ANC combinations of one measurement sample can be described with the following matrix forms:

$$\mathbf{J} = \begin{bmatrix} \frac{\partial f_1}{\partial x} & \frac{\partial f_1}{\partial y} \\ \frac{\partial f_2}{\partial x} & \frac{\partial f_2}{\partial y} \\ \vdots & \vdots \\ \frac{\partial f_N}{\partial x} & \frac{\partial f_N}{\partial y} \end{bmatrix}, \qquad \mathbf{f} = \begin{bmatrix} f_1 \\ f_2 \\ \vdots \\ f_N \end{bmatrix}$$

The Newton non-linear least squares minimization method is expressed by:

$$\mathbf{x}_{k+1} = \mathbf{x}_k - \left(\mathbf{J}_k^T \mathbf{J}_k\right)^{-1} \mathbf{J}_k^T \mathbf{f}_k \tag{3.9}$$

This is an iterative process. Each result, designated by $\{k + 1\}$, is used in the next repetition of equation 3.9. This process stops when the desired accuracy has been achieved which makes it relatively slow.

## 3.3 Larsson algorithm

In 2019 Larsson published a paper [16] that formulates optimal trilateration as an eigenvalue problem. This approach is expected to have a reduced computational load compared to the iterative non-linear least-squares optimization by Murphy. In this section, a specific part of the Larsson localization approach is explained concerning ToA.

We want to estimate the unknown location of a TAG $\mathbf{x}\epsilon\mathbb{R}^n$. Here $n$ is the number of dimensions. The position is recovered by measuring the distance between the TAG (black cross) and an ANC designated by a blue triangle.

A typical trilateration case aims to have $||\mathbf{x} - \mathbf{a}_j||^2 = d_j$ for $j = 1, 2, ..., N$ which are the number of ANCs. For these type of situations the following cost function is often used:

$$\sum_{j=1}^{N} \left(||\mathbf{x} - \mathbf{a}_j|| - d_j\right)^2$$

These types of problems can have multiple local minima. An alternative cost function for trilateration is formulated:

$$h_1(\mathbf{x}) = \sum_j \frac{1}{4d_j^2} \left(||\mathbf{x} - \mathbf{a}_j||^2 - d_j^2\right)^2 \tag{3.10}$$

The difference in this formulation is the fourth-order formulation with a normalization factor $w_j = \frac{1}{4d_j^2}$ which can be written in the form:

$$h(\mathbf{x}) = \sum_j w_j \left(\mathbf{x}^T\mathbf{x} - 2\mathbf{x}^T\mathbf{a}_j + \mathbf{a}_j^T\mathbf{a}_j - d_j^2\right)^2 \tag{3.11}$$

Equation 3.11 is differentiable everywhere. The globally optimal solution must lie at a point where:

$$\nabla h(\mathbf{x}) = 4\sum_j w_j \left(\mathbf{x}^T\mathbf{x} - 2\mathbf{x}^T\mathbf{a}_j + \mathbf{a}_j^T\mathbf{a}_j - d_j^2\right)(\mathbf{x} - \mathbf{a}_j) = 0 \tag{3.12}$$

This gives a polynomial equation with a degree of three. The next step is to write out equation 3.12 and to collect the terms in their respective degrees (e.g. equation 3.13 has the degree of 3, and equation 3.14 the degree of 2 upto equation 3.16):

$$\frac{1}{4}\nabla h(\mathbf{x}) = \left(\sum_j w_j\right)\left(\mathbf{x}^T\mathbf{x}\right)\mathbf{x} \tag{3.13}$$

$$-\left(\mathbf{x}^T\mathbf{x}\mathbf{I} + 2\mathbf{x}\mathbf{x}^T\right)\left(\sum_j w_j\mathbf{a}_j\right) \tag{3.14}$$

$$+\left(\sum_j w_j\left(\mathbf{a}_j^T\mathbf{a}_j - d_j^2\right)\mathbf{I} + 2\mathbf{a}_j\mathbf{a}_j^T\right)\mathbf{x} \tag{3.15}$$

$$+\sum_j w_j\left(d_j^2 - \mathbf{a}_j^T\mathbf{a}_j\right)\mathbf{a}_j = 0 \tag{3.16}$$

These terms can be simplified with the following assumptions. The ANCs $\mathbf{a}_j$ have known locations that are expressed in an arbitrary coordinate system. These locations can be translated to a for this problem optimal location:

$$\mathbf{t} = \frac{\left(\sum_j w_j\mathbf{a}_j\right)}{\left(\sum_j w_j\right)} \tag{3.17}$$

This equation makes the factor $\sum_j w_j\mathbf{a}_j = 0$, and leads to the cancellation of equation 3.14. Another simplification is the observation that the weights of the cost function are homogeneous. Then it can be assumed without loss of generality that $\sum_j w_j = 1$. That makes all the coefficients of equation 3.13 equal to 1. These assumptions combined give a simpler form of equation 3.12:

$$\left(\mathbf{x}^T\mathbf{x}\right)\mathbf{x} + \mathbf{A}\mathbf{x} + \mathbf{b} = 0 \tag{3.18}$$

The matrix $\mathbf{A}$ in equation 3.18 is symmetric (because the $2\mathbf{a}_j\mathbf{a}_j^T$ term in equation 3.15), which allows it to be decomposed with the orthogonal eigenvalue decomposition: $\mathbf{A} = \mathbf{U}\mathbf{D}\mathbf{U}^\mathbf{T}$. Based on the decomposition an advantageous change of variables can be performed: $\mathbf{x} \to \mathbf{U}\mathbf{x}$ and $\mathbf{b} \to \mathbf{U}\mathbf{b}$ which lead to:

$$\left((\mathbf{U}\mathbf{x})^T\mathbf{U}\mathbf{x}\right)\mathbf{U}\mathbf{x} + \mathbf{U}\mathbf{D}\mathbf{U}^\mathbf{T}\mathbf{U}\mathbf{x} + \mathbf{U}\mathbf{b} = 0 \tag{3.19}$$

The multiplication of an orthogonal matrix with its transpose gives the identity matrix which simplifies equation 3.19 to:

$$\mathbf{U}\left(\left(\mathbf{x}^T\mathbf{x}\right)\mathbf{x} + \mathbf{D}\mathbf{x} + \mathbf{b}\right) = 0 \tag{3.20}$$

Now, two factors can be zero, the matrix $U$ or the factor $\left(\mathbf{x}^T\mathbf{x}\right)\mathbf{x} + \mathbf{D}\mathbf{x} + \mathbf{b}$. This allows to work with one or the other, in this case the latter.

Next, equation 3.20 is written in the following form:

$$\left(\mathbf{x}^T\mathbf{x}\right)x_i + D_{ii}x_i + b_i = 0, \quad i = 1, 2, ..., n \tag{3.21}$$

This is allowed as $\mathbf{x}^T\mathbf{x}$ is a constant and $D$ is a diagonal matrix, and a value on the diagonal can be written as $D_{ii}$. A value from the vector $\mathbf{b}$ is written as $b_i$. The goal of this set of conversions is to write the equation in an eigenvalue problem form. A first step is multiplying equation 3.21 by $x_i$, giving:

$$\left(\mathbf{x}^T\mathbf{x}\right)x_i^2 + D_{ii}x_i^2 + b_ix_i = 0, \quad i = 1, 2, ..., n \tag{3.22}$$

The vector of squares as used in equation 3.22 can be written as: $\mathbf{x}_*^2 = (x_1^2, x_2^2, ..., x_n^2)^T$ and the same goes for $\mathbf{x}_* = (x_1, x_2, ..., x_n)^T$. Here the notation is abused compared to previous section, but this allows to better discriminate the form in equation 3.23. Finally, to get the desired eigenvalue form equation 3.21 and equation 3.22 are combined:

$$(\mathbf{x}^T\mathbf{x})\begin{bmatrix}\mathbf{x}_*^2\\ \mathbf{x}_*\\ \mathbf{1}\end{bmatrix} = \begin{bmatrix}-D & -diag(\mathbf{b}) & \mathbf{0}\\ \mathbf{0} & -D & -\mathbf{b}\\ \mathbf{1}^T & \mathbf{0}^T & 0\end{bmatrix}\begin{bmatrix}\mathbf{x}_*^2\\ \mathbf{x}_*\\ \mathbf{1}\end{bmatrix} \tag{3.23}$$

Please note that the last row of equation 3.23 is an arbitrary equality. Equation 3.23 can be interpreted as an eigenvalue problem of the familiar form:

$$\lambda\mathbf{v} = \mathbf{M}\mathbf{v} \tag{3.24}$$

In this case every solution to equation 3.23 must be a solution to equation 3.12. The right eigenvector contains, amongst others, the location of the TAG. To get the location of the TAG the following steps must be executed:

1. Compute matrix $\mathbf{M}$
2. Compute all its eigenvectors (each one containing a candidate for the best fitting location of the TAG
3. Normalize all the eigenvectors so that the last element is equal to one. This is done because the last element of the vector in equation 3.23 is also one
4. Use equation 3.12 to find the best candidate by iterating over all eigenvectors

The last step guarantees to find the global optimal solution[1].

This approach is faster than Murphy because it consists of a lower amount of calculations that are computationally more efficient. But some iteration is still present in Larsson. For instance, the calculations of eigenvalues are, internally, often done

[1] This solution still requires extra care in case of colinear ANCs.

iteratively. Next to that, all eigenvectors have to checked with equation 3.23. But this number of iterations is constant assuming that the number of ANCs does not change.

## 3.4 Faber algorithm

During the analysis of Larsson and Murphy, a collaboration started with H. Faber (The Hague University of Applied Sciences). Inspired by Larsson, an attempt was made to find a better trilateration algorithm. The Faber algorithm was conceived by H. Faber and tested and simulated by the author.

The sum of the squared distances between an ANC and TAG should be close to the sum of the measurement distances:

$$\sum_{j=1}^{N} ||\mathbf{x} - \mathbf{a}_j||^2 = \sum_{j=1}^{N} \tilde{d_j}^2 \tag{3.25}$$

This was formulated to minimize the error, and it was simulated and concluded that the constraint equation 3.25 could be too strict. Equation 3.26 shows a relaxation of that constraint:

$$\sum_{j=1}^{N} ||\mathbf{x} - \mathbf{a}_j||^2 = R_{tot} \tag{3.26}$$

Here $R_{tot}$ is one of the variables that has to be calculated. Expand equation 3.26:

$$\sum_{j=1}^{N} x^2 + a_{x,j}^2 - 2x \cdot a_{x,j} + a_{y,j}^2 + y^2 - 2a_{y,j} \cdot y = R_{tot} \tag{3.27}$$

This can further be expanded to:

$$N \cdot x^2 + N \cdot y^2 + \sum_{j=1}^{N} a_{x,j}^2 + \sum_{j=1}^{N} a_{y,j}^2 - \sum_{j=1}^{N} 2 \cdot x \cdot a_{x,j} - \sum_{j=1}^{N} 2 \cdot y \cdot a_{y,j} = R_{tot} \tag{3.28}$$

Collect and isolate the desired position:

$$x^2 + y^2 = \frac{2 \cdot x \cdot \sum_{j=1}^{N} a_{x,j} + 2 \cdot y \cdot \sum_{j=1}^{N} a_{y,j} + R_{tot} - \sum_{j=1}^{N} a_{x,j}^2 - \sum_{j=1}^{N} a_{y,j}^2}{N} \tag{3.29}$$

Based on figure 3.1 a range measurement, the circle equation can be formulated as:

$$(x - a_{x,j})^2 + (y - a_{y,j})^2 = \tilde{d_j}^2 \tag{3.30}$$

Expanding and reordering gives:

$$x^2 + y^2 + a_{x,j}^2 - 2 \cdot x \cdot a_{x,j} + a_{y,j}^2 - 2 \cdot y \cdot a_{y,j} = \tilde{d_j}^2 \tag{3.31}$$

The same terms are present in equation 3.29 and in equation 3.31 and so the equations can be combined via substitution:

$$\frac{2 \cdot x \cdot \sum_{j=1}^{N} a_{x,j} + 2 \cdot y \cdot \sum_{j=1}^{N} a_{y,j} + R_{tot} - \sum_{j=1}^{N} a_{x,j}^2 - \sum_{j=1}^{N} a_{y,j}^2}{N} + a_{x,j}^2 - 2 \cdot x \cdot a_{x,j} + a_{y,j}^2 - 2 \cdot y \cdot a_{y,j} = \tilde{d_j}^2 \tag{3.32}$$

This equation is linear for $x$, $y$ and $R_{tot}$ and be written in the following form:

$$\left(\frac{2\cdot\sum_{j=1}^{N} a_{x,j}}{N} - 2\cdot a_{x,j}\right)\cdot x + \left(\frac{2\cdot\sum_{j=1}^{N} a_{y,j}}{N} - 2\cdot a_{y,j}\right)\cdot y + \frac{1}{N}\cdot R_{tot} = \tilde{d_j}^{\,2} + \frac{\sum_{j=1}^{N} a_{x,j}^2 + \sum_{j=1}^{N} a_{y,j}^2}{N} - a_{x,j}^2 - a_{y,j}^2 \tag{3.33}$$

This can be written in matrix form:

$$\begin{bmatrix} \frac{2\cdot\sum_{j=1}^{N} a_{x,j}}{N} - 2\cdot a_{x,1} & \frac{2\cdot\sum_{j=1}^{N} a_{y,j}}{N} - 2\cdot a_{y,1} & \frac{1}{N} \\ \frac{2\cdot\sum_{j=1}^{N} a_{x,j}}{N} - 2\cdot a_{x,2} & \frac{2\cdot\sum_{j=1}^{N} a_{y,j}}{N} - 2\cdot a_{y,2} & \frac{1}{N} \\ \vdots & & \\ \frac{2\cdot\sum_{j=1}^{N} a_{x,j}}{N} - 2\cdot a_{x,N} & \frac{2\cdot\sum_{j=1}^{N} a_{y,j}}{N} - 2\cdot a_{y,N} & \frac{1}{N} \end{bmatrix} \begin{bmatrix} x \\ y \\ R_{tot} \end{bmatrix} = \begin{bmatrix} \tilde{d_1}^{\,2} - a_{x,1}^2 - a_{y,1}^2 + \frac{\sum_{j=1}^{N} a_{x,j}^2 + \sum_{j=1}^{N} a_{y,j}^2}{N} \\ \tilde{d_2}^{\,2} - a_{x,2}^2 - a_{y,2}^2 + \frac{\sum_{j=1}^{N} a_{x,j}^2 + \sum_{j=1}^{N} a_{y,j}^2}{N} \\ \vdots \\ \tilde{d_N}^{\,2} - a_{x,N}^2 - a_{y,N}^2 + \frac{\sum_{j=1}^{N} a_{x,j}^2 + \sum_{j=1}^{N} a_{y,j}^2}{N} \end{bmatrix} \tag{3.34}$$

Which has the well known form:

$$\mathbf{Ax} = \mathbf{b} \tag{3.35}$$

As the last step, the $\mathbf{A}$ matrix[2] are normalized by dividing each row by their associated distance squared. This normalization gave the best results in practice. An explanation can be that the combination of equation 3.29 and equation 3.31 both predominantly contain terms that are squared. The weight matrix is given by:

$$\mathbf{W} = \begin{bmatrix} \frac{1}{\tilde{d_1}^{\,2}} & 0 & 0 \\ 0 & \frac{1}{\tilde{d_2}^{\,2}} & 0 \\ & \vdots & \\ 0 & 0 & \frac{1}{\tilde{d_N}^{\,2}} \end{bmatrix} \tag{3.36}$$

Then the matrix equation becomes:

$$\mathbf{WAx} = \mathbf{Wb} \tag{3.37}$$

Equation 3.37 is tested in section 6.1 with Matlab R2020a. The measurements done in this project are based on a setup consisting of four ANCs which gives an overdetermined set of equation in the Faber case. In the overdetermined case where $\mathbf{A}\epsilon\mathbb{R}^{n\times m}$ with $n > m$ Matlab uses a QR-solver [3] which gives a least-squares approximation. This means that Murphy, Larsson and Faber all give results in the least-squares sense.

[2] In this case not explicitly designated.
[3] see https://nl.mathworks.com/help/matlab/ref/mldivide.html.

The Faber localization algorithm has the least amount of calculations compared to Murphy and Larsson. This most likely makes the Faber solution the fastest of them all.

## 3.5 UWB error modeling

Noise is often simulated by adding a Gaussian Random Variable to the coordinates. Gaussian noise, opposed to other types of noise, tends to give tractable solutions [40]. However, in UWB localization, noise is not necessarily a Gaussian Random Variable.

In the work of Alavi et. al. [4] the authors try to introduce an empirically established statistical model for UWB distance measurement errors and finally arrive at:

$$\epsilon_{M,W}(d) = \gamma_W log(1+d) = G(m_{W,M}, \sigma_{M,W}) log(1+d) \tag{3.38}$$

The mean $m_{M,W}$ and the variance $\sigma^2_{M,W}$ is given by Alavi et. al. in a table containing the typical values for different *Bandwidth*s (BWs). The UWB error distance dependency is aligned with the results in other similar work [54]. This is applied to the localization algorithms in this work to get more realistic UWB noise.

# Chapter 4

# Sensor fusion

The goal of this project is to improve the localization of wheelchair athletes. The current system, the *Wheelchair Mobility Performance Monitor* (WMPM) is solely based on *Inertial Measurement Unit*s (IMUs) and does not provide absolute coordinates. *Ultra-wideband* (UWB) is chosen as the technology to improve this. The WMPM has a relatively high precision (figure 4.2) and a relatively low accuracy. The UWB data has a relatively high accuracy (figure 4.3) but a relatively low precision. Combining these systems should improve the overall precision and accuracy.

## 4.1 Overview

For sensor fusion, we consider three coarsely defined options: the *Kalman Filter* (KF) and the *Particle Filter* (PF) and a combination thereof [6]. As stated in section 4.2 the obtained measurement data is non-linear which eliminates the standard KF and suggests the use of a non-linear KF: the *Extended Kalman Filter* (EKF) or the *Unscented Kalman Filter* (UKF). The particle filter is less suitable as a solution due to the associated computational loads.

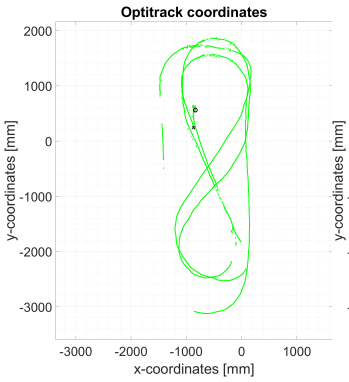


**Figure 4.1:** Groundtruth data (Optitrack). Note the parts in the missing data.

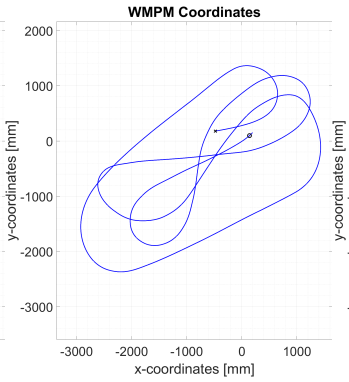


**Figure 4.2:** Relative location from the WMPM.

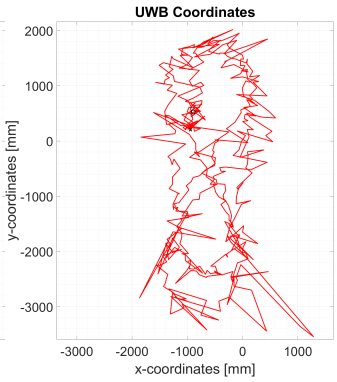


**Figure 4.3:** UWB data, simultaneously acquired with figure 4.1 and figure 4.2.

Typically, the KF is used for optimal estimation under the assumption of linearity and Gaussian disturbance. But is also often used for sensor fusion [13, 30, 42, 6].

In the sensor fusion solution, as can be seen in figure 4.4, the data from UWB and IMUs serves as input. The WMPM is used as a form of preprocessing of IMU data and outputs the frame velocity $\tilde{v_k}$. A tilde symbol represents a measured value from

the IMUs. A hat symbol, on the other hand, represents a variable from the state vector after filtering. The subscript $k$ designates the k-th discrete timestep. The wheelchair frame IMU, part of the WMPM setup, will be used for its rotational velocity $\tilde{\dot{\theta}}_k$ output in the horizontal plane[1]. The IMUs together, provide the frame velocity $\tilde{v_k}$. UWB provides an estimation of the true position $x_k$ and $y_k$ which again has a similar notation as in chapter 3. Together, these outputs serve as the input for sensor fusion and filtering and give absolute pose $(\hat{x_k}, \hat{y_k}, \hat{\theta}_k)$ tracking. The sensor fusion output will be evaluated in comparison to the ground truth (Optitrack) which gives the coordinates $x_k^*, y_k^*$. Lastly, some state variables are not measured, but they are still an output of the UKF. They are called 'hidden state variables' as they are not observed.

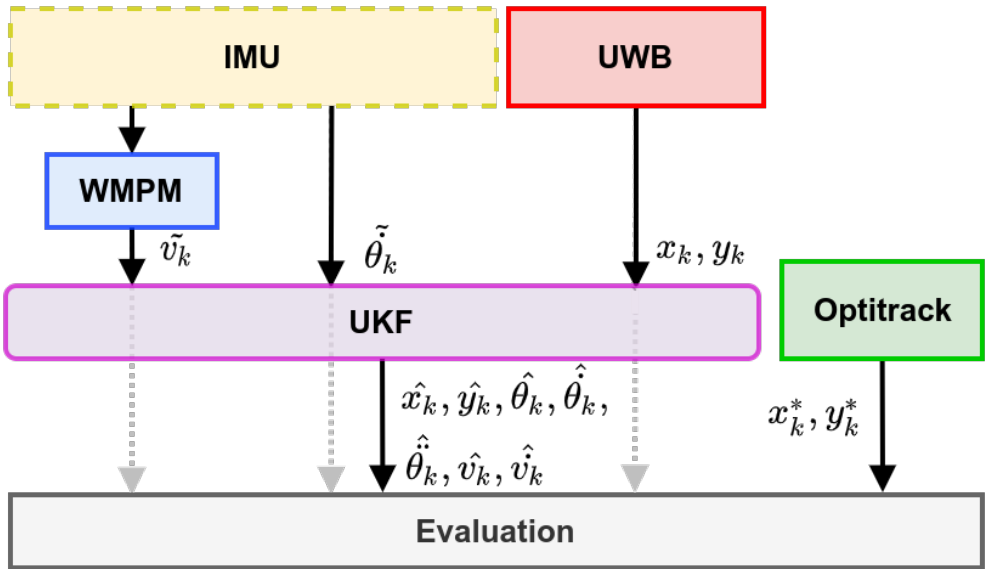


**Figure 4.4:** Schematic overview of sensor fusion. Similar to chapter 3 a measured value is indicated with a tilde. It illustrates the type of data obtained from the systems that serve as input for the sensor fusion (UKF). The UKF returns the state variable (indicated with a hat, e.g. $\hat{x_k}$. Note that the UKF also returns quantities not directly measured, the so-called 'hidden state variables'. The Optitrack data is used for evaluation purposes.

## 4.2 Non-linear measurement data

In figure 4.1, figure 4.2 and figure 4.3 an example is shown of simultaneous measurements done with respectively the Optitrack system, WMPM system and the UWB system. Please note that in figure 4.1 there is some missing data. This is due to a too low Optitrack camera density and a sub-optimal TAG placement with regards to Optitrack marker visibility. It can be seen that the data is non-linear. A KF is based on the assumption that the movement model $\mathbf{F}$ is linear and that the measurement data $\mathbf{z}$ is also linear. To deal with non-linearities in the KF the respective covariance values $\mathbf{Q}$, $\mathbf{R}$ are increased. This means that non-linearities are interpreted as a disturbance. During the development phase, this was shown not to be sufficient.

In general, there are two non-linear KF implementations the EKF and the UKF. The literature suggests that the UKF is the better choice for implementation and performance reasons [52, 53, 14].

[1] The dot in $\dot{[]}$ represents the first derivative.

## 4.3 Kalman Filter description

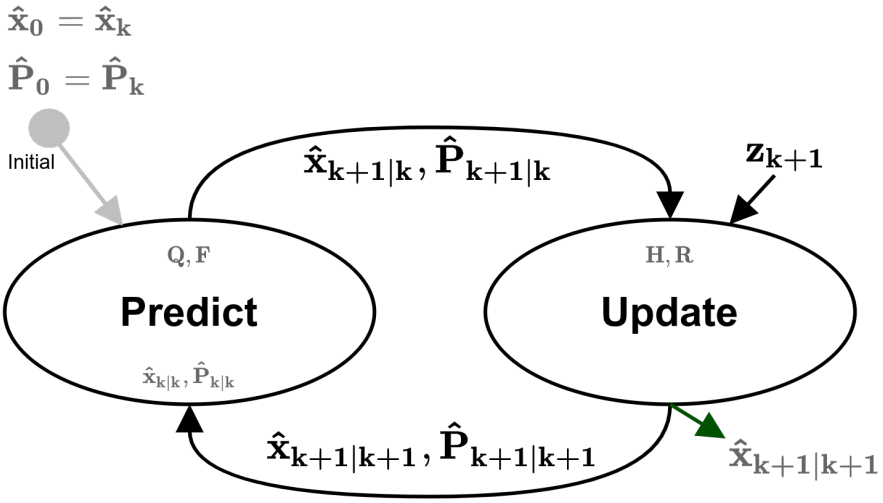


**Figure 4.5:** The schematic proces of the Kalman Filter for comparison with the Unscented Kalman Filter.

To understand the UKF a good start is the KF, which is briefly covered in this subsection. A state vector $\mathbf{x}$ is defined based on the variables that can be tracked and that are needed:

$$\mathbf{x} = \begin{bmatrix} x & y & \theta & \dot{\theta} & \ddot{\theta} & v & \dot{v} \end{bmatrix}^T \tag{4.1}$$

Also the covariance matrix $\mathbf{P}$ is update every iteration. The covariance matrix $\mathbf{P}$ contains the (co)variance(s) of each state variable and can be seen as the *uncertainty* of each variable. Here, a high variance for a certain state variable, means a high uncertainty in the predict phase and more weight is given to the measurement value in the update phase.

The linear KF consists of two phases: the *predict* phase and the *update* phase as schematically visualized in figure 4.5. In the predict phase, a movement model $\mathbf{F}$, also called transition matrix, is used to predict the next state vector $\mathbf{x}_{k+1|k}$ as seen in equation 4.2.

$$\hat{\mathbf{x}}_{\mathbf{k+1|k}} = \mathbf{F}\hat{\mathbf{x}}_{\mathbf{k|k}} \tag{4.2}$$

$$\hat{\mathbf{P}}_{\mathbf{k+1|k}} = \mathbf{F}\hat{\mathbf{P}}_{\mathbf{k|k}}\mathbf{F}^{\mathbf{T}} + \mathbf{Q} \tag{4.3}$$

Also, the covariance matrix is calculated based on the movement model and the previous values the *process noise* $\mathbf{Q}$ is added which signifies the uncertainty of the process model. Each discrete timestep $k$ the discrete linear KF executes these two phases. Here subscript $k{+}1|k$ represents the output of the predict phase with subscript $k+1$ **given** the state vector from the previous timestep $k$. This is called the *prior*, i.e. the state vector after the 'predict' phase. After the update phase, the subscripts of the state vector and covariance matrix change to $k+1|k+1$.

Because the prediction does not have any information about the true state, measurement information has to be incorporated to 'update' the state vector. This is done in the update phase with the measurement data represented by the vector $\mathbf{z}$, the *observation* vector. This vector $\mathbf{z}$ must be transformed, so it is similar formatted as the state vector $\mathbf{x}$. This is done by multiplying the *measurement* function $\mathbf{H}$ with the state vector, which is used to calculate the *residual* vector $\mathbf{y}$ in equation 4.4.

$$\mathbf{y}_{\mathbf{k+1|k+1}} = \mathbf{z}_{\mathbf{k+1}} - \mathbf{H}\mathbf{x}_{\mathbf{k+1|k}} \tag{4.4}$$

In the predict phase, given an initial or previous state vector $\hat{\mathbf{x}}_{\mathbf{k|k}}$ and the corresponding covariance matrix $\mathbf{P}_{\mathbf{k|k}}$, a prediction can be made, see equation 4.2 and equation 4.3. The next step is to calculate the *Kalman gain* $\mathbf{K}$ as seen in equation 4.6. First the *system uncertainty* $\mathbf{S}$ is calculated which uses the *measurement noise* $\mathbf{R}$ in equation 4.5. The measurement noise is difficult to obtain as sensor manufacturers often forget to specify the sensor noise. In a typical KF implementation the measurement noise is estimated and then tuned for a specific goal.

$$\mathbf{S} = \mathbf{H}\hat{\mathbf{P}}_{\mathbf{k+1|k}}\mathbf{H}^{\mathbf{T}} + \mathbf{R} \tag{4.5}$$

$$\mathbf{K} = \hat{\mathbf{P}}_{\mathbf{k+1|k}}\mathbf{H}^{\mathbf{T}}\mathbf{S}^{-\mathbf{1}} \tag{4.6}$$

Finally, $\mathbf{K}$ is used to calculate the *posterior* state vector $\hat{\mathbf{x}}_{\mathbf{k+1|k+1}}$ and *posterior* covariance $\hat{\mathbf{P}}_{\mathbf{k+1|k+1}}$ as seen in equation 4.7 and equation 4.8 which will serve again as input for the prediction phase [2]. These quantities are called the *posterior* [3].

$$\hat{\mathbf{x}}_{\mathbf{k+1|k+1}} = \hat{\mathbf{x}}_{\mathbf{k+1|k}} + \mathbf{K}\mathbf{y}_{\mathbf{k+1|k+1}} \tag{4.7}$$

$$\hat{\mathbf{P}}_{\mathbf{k+1|k+1}} = (\mathbf{I} - \mathbf{KH})\hat{\mathbf{P}}_{\mathbf{k+1|k}} \tag{4.8}$$

## 4.4 The Unscented Kalman Filter

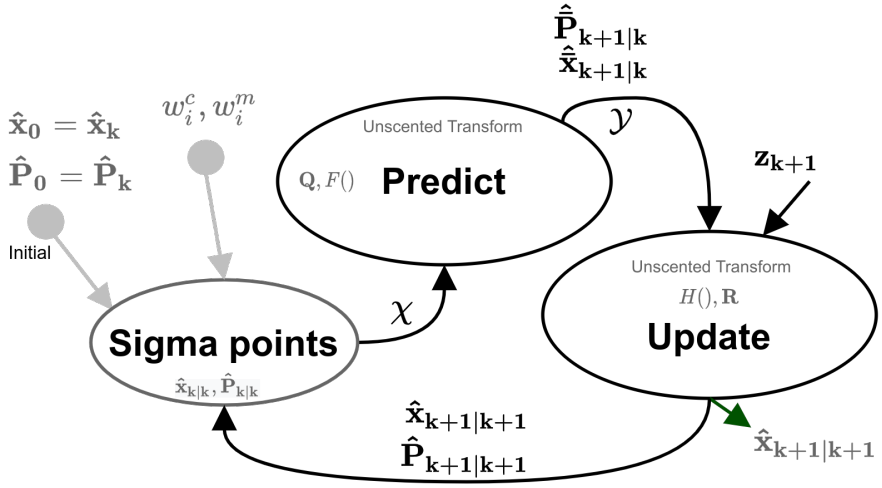


**Figure 4.6:** The schematic UKF. It consists of a couple of additions compared to the Kalman filter figure 4.5.

In figure 4.6 the UKF is schematically represented. The idea behind the UKF is that it is easier to approximate a model with samples, than to approximate a non-linear function for instance with a EKF. The samples, called 'sigma-points', sample the non-linear model to represent it as good as possible with as few samples as possible. For instance, if a certain state variable is very non-linear (e.g. the coordinate $x_k$), only one sample of that state variable will likely give a bad prediction. Multiple samples, a distribution, will give a better representation of the non-linear behavior.

[2] In that transition from *update* output to *predict* input the subscripts change from $\hat{\mathbf{x}}_{\mathbf{k+1|k+1}}$ to $\hat{\mathbf{x}}_{\mathbf{k|k}}$.
[3] Which can be interpreted as 'after the update phase'.

Each 'sigma-point prediction' of a state variable will be compared to the measurement value in the update phase and the best fitting will be used. This is how an UKF deals with non-linearities.

In this project, the sigma points are obtained via the method of van der Merwe [43]. The sigma points $\boldsymbol{\chi}$ are picked in such a way that their sample mean is similar to $\hat{\mathbf{x}}$ and $\hat{\mathbf{P}}$. Then each consecutive sigma point is an input to $\mathbf{F}()$ which gives a set of transformed points $\boldsymbol{\mathcal{Y}}$ called the *prior sigma points*. The prior sigma points are used in the update phase to calculate the best possible representation of the state vector and covariance matrix. A mathematical description of the UKF is given in section B.4. An important distinction with a Monte Carlo-type method, like the PF, is that the set of points or samples are in the UKF given by a deterministic algorithm.

### 4.4.1 Measurement function and motion model

This section describes the measurement function and the motion model. The state vector $\mathbf{x}$ is expressed in equation 4.1.

The measurement vector for UWB $\mathbf{z}_{UWB}$ is:

$$\mathbf{z}_{UWB} = \begin{bmatrix} \hat{x} & \hat{y} \end{bmatrix}^T \tag{4.9}$$

The measurement vector for IMU $\mathbf{z}_{IMU}$ is:

$$\mathbf{z}_{IMU} = \begin{bmatrix} \hat{v} & \hat{\dot{\theta}} \end{bmatrix}^T \tag{4.10}$$

Every timestep (or iteration) the state vector and covariance need to be predicted. In this discrete Kalman implementation every timestep $k$ has an assumed duration of $dt$:

$$F = \begin{bmatrix} x_k + v_k \cdot cos(\theta_k) \cdot dt + v_k \cdot cos(\theta_k) \cdot 0.5 \cdot dt^2 \\ y_k + v_k \cdot sin(\theta_k) \cdot dt + v_k \cdot sin(\theta_k) \cdot 0.5 \cdot dt^2 \\ \theta_k + \dot{\theta}_k \cdot dt + 0.5 \cdot \ddot{\theta_k} \cdot dt^2 \\ \dot{\theta}_k + \ddot{\theta} \cdot dt \\ \ddot{\theta}_k \\ v_k + \dot{v}_k \cdot dt \\ \dot{v}_k \end{bmatrix} \tag{4.11}$$

In the movement model, the wheelchair velocity $\tilde{v}$ from the WMPM is used to give a magnitude to the state variables $x_k$ and $y_k$. The rotational velocity $\tilde{\dot{\theta}}$ is used to determine the hidden state variable $\hat{\theta}$, the angle or orientation of the TAG. This state variable $\hat{\theta}$, combined with $\tilde{v}$ is used to determine the change of $x_k$ and $y_k$ in one timestep.

### 4.4.2 Multi-rate sensor fusion

The WMPM and UWB systems operate at different update rates, such combinations of systems are called multi-rate systems. In this specific UKF implementation the fastest sensor determines the timing resolution $dt$. At every timestep $k$ the slower sensors are checked for new data. If new data from a slower sensor is available, then the update phase is executed specifically for that sensor. In one iteration $k$ the update phase can be executed two times, one for each sensor.

This has the disadvantage of *offsetting* the data and reducing the precision (the data becomes 'jumpy'). The reduced precision is caused by the difference in update rate of the sensors and the fact that the sensors 'update' different state variables. This is illustrated in figure 4.7 which shows two simulations with different update rates.

The offsetting and inprecision increases with the difference in update-rate which is shown in figure 4.7 **a** and **b**. At the start of a measurement, a location offset is obtained related to the UWB variance. This offset is slowly recovered due the relatively low localization update rate.

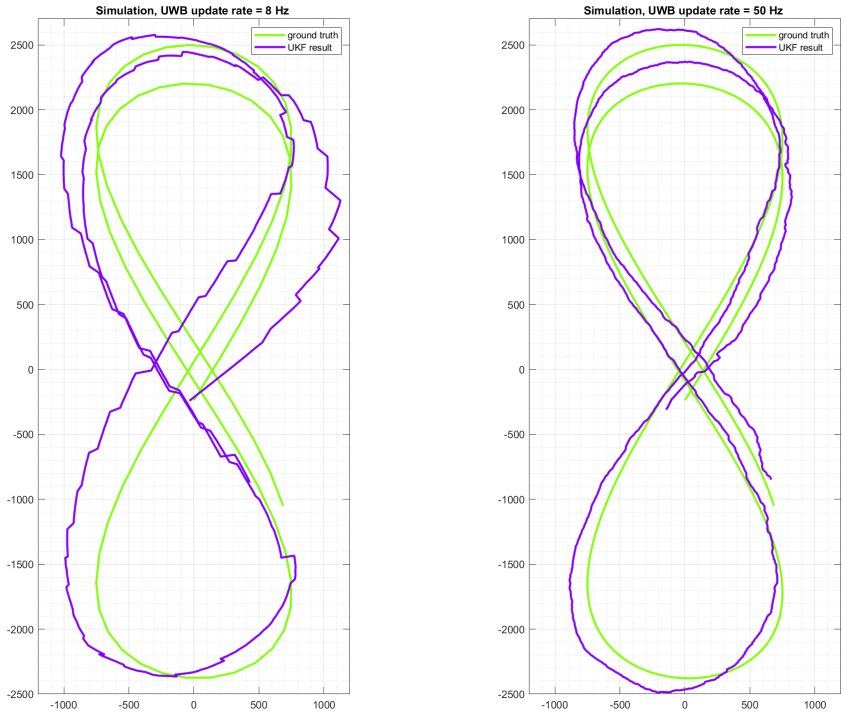


**Figure 4.7:** The simulated effect on the output of the UKF by combining multi-rate sensors at different updates rates. In **a** the simulated update rate ($8Hz$) is similar to the update rate in UWB. In **b** the simulated update rate is $50Hz$.

These simulations support the statement that the update rate of the used systems should be as high as possible. A lower update rate will increase a potential offset and make the result less precise.

## 4.5 Rauch-Tung-Striebel Smoother

To 'smooth' the offsetting and reduced precision the 'Rauch-Tung-Striebel' smoother is applied, named after the authors [31], and abbreviated with RTS. There is a difference between *filtering* and *smoothing*. Filtering is considered as the *forward pass* over the data, i.e. the KF. Smoothing is the *backward pass* over the data, also considering future data, a form of batch processing. Kalman smoothers provide the best estimate as they incorporate all past and future data. Smoothing is more computationally intensive but also comes with considerable advantages:

- It can handle missing values better
- It provides better estimates of the state vector
- It provides a better estimate of the covariance

### 4.5.1 Types of KF smoothers

There are three types of smoothing implementations of which one could be used in a real-time solution. The **Fixed-interval** is the batch-processing variant of the RTS-smoother and will process all available data. In this work, a **Fixed-interval** type of smoothing is applied.

A **Fixed-lag** type will introduce a *fixed-lag* into the output. For instance, at timestep $k$, $n$ number of update frames are awaited. Then at timestep $k$ all the previously collected samples $k-n...k$ and the corresponding KF state vector and covariances) will be taken into account. These types of smoothers can be used in real-time systems.

A **Fixed-point** smoother uses all measurements from a timestep $k$ up to a timestep $k+n$ to accurately determine the state at timestep $k$. This is useful when, for instance, an initial state of a system needs to be accurately determined.

### 4.5.2 RTS Implementation

The RTS smoother continues with the UKF data and works backward from the timestep $N-1$ to the first sample. This way 'future' data is incorporated in the calculation of the state vector and the covariance. The mathematical steps are given in section B.5.

# Chapter 5

# Measurement setup

The main goal of the measurements is to test the localization algorithms in an UWB setting and to have a dataset for development of a sensor fusion solution. To evaluate the accuracy of the algorithms, the Optitrack system was used as the ground truth. The measurement setup consisted of:

- An Optitrack System with 20 Flex13 camera's
- The Pozyx Creator UWB System which had four TAGs and four *Anchor*s (ANCs) and uses *Two Way Ranging* (TWR)
- An RC-Car, for *Line-Of-Sight* (LoS) measurements as seen in figure 5.3
- A Wheelchair, a seen in figure 5.4, for simultaneous measurement with the WMPM.
- An custom electronic setup consisting that provided synchronization of the different measurement systems figure 5.1
- A computer with Motive version 2.2.0 Final (Optitrack operational software).

This is visualized in figure 5.1 in which the red dots illustrate the space where the Opitrack markers can be tracked. UWB data was obtained with the Pozyx Creator system. The Pozyx system is used due to its robustness, maturity, reproducibility and ease-of-use.

Optitrack and UWB were automatically synchronized with a custom solution (see: figure 5.1). The solution was used to start and stop UWB measurements and simultaneously turn on a set of Optitrack compatible IR-LEDs which could be automatically recognized in the post-processing.

UWB can, besides ranging, be used to transmit information. In the setup, as shown in figure 5.1, UWB is also used to transmit the ranges from the TAG to the computer.

## 5.1 UWB and Optitrack combination

Figure 5.2 shows that the UWB ANCs had Optitrack markers mounted to them. Each ANC has a specific Optitrack marker layout, to uniquely define that UWB antenna in the Optitrack data. The UWB antenna chip, the white chip with the blue square in figure 5.2 between the lower two Optitrack markers, is considered the point of origin for ranging.

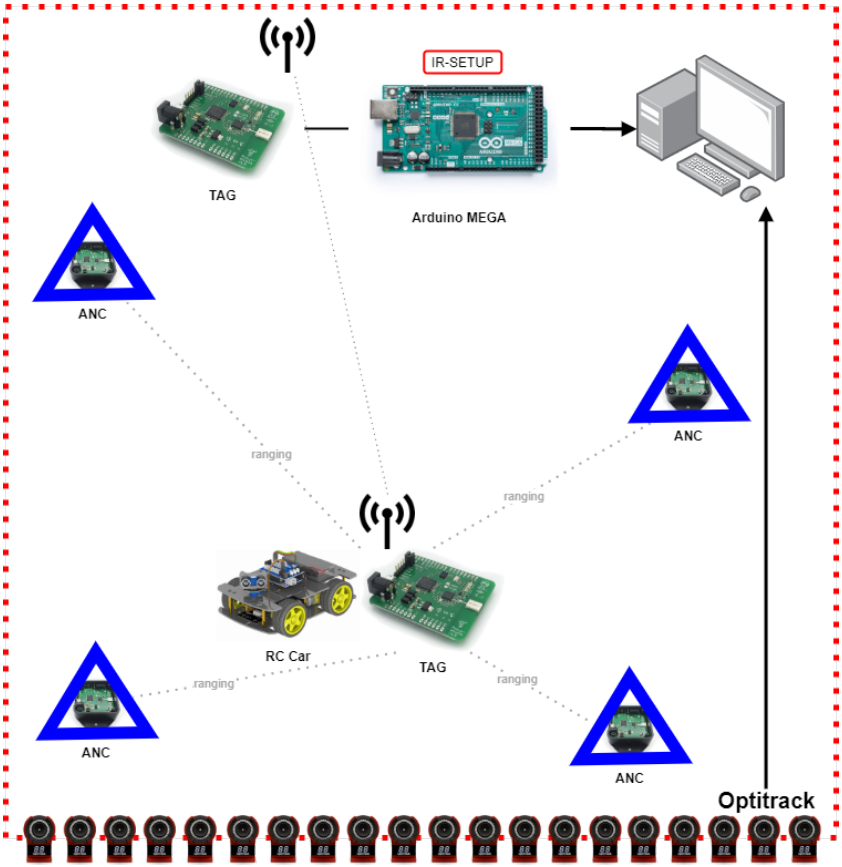


**Figure 5.1:** The global measurement setup. During the measurements 4 ANCs were available and 4 TAGs. One TAG was used for the streaming of data via an Arduino. That Arduino also had an electronic board for synchronization with a fixed configuration of 3 850nm IR-LEDS.

## 5.2 WMPM

The WMPM consists of three IMUs shown in figure 5.5. One IMU is placed on the wheel close to the axis of rotation. Another IMU is placed on the base of the wheelchair. The last IMU measured the movements of the athlete and was placed on the seat and ignored.

The IMUs are made by a company called Movesense and consist of the LSM6DS3 IMU that has an 3D accelerometer and 3D gyroscope. The WMPM version used in the measurements, did not output accelerometer data for throughput reasons. This means that no wheelchair acceleration data is used, which would otherwise provide extra input for the sensor fusion solution.

## 5.3 Measurements

Three types of measurements were recorded for 3 days:

- Static and dynamic ranging measurements (to test the localization algorithms)
- Static and dynamic localization measurements, based on a proprietary Pozyx algorithm for comparison with the localization algorithms used in this project.
- Static and dynamic ranging combined with WMPM for sensor fusion chapter 4. In every measurement at least 2 wheel slip moments are added to introduce noise.

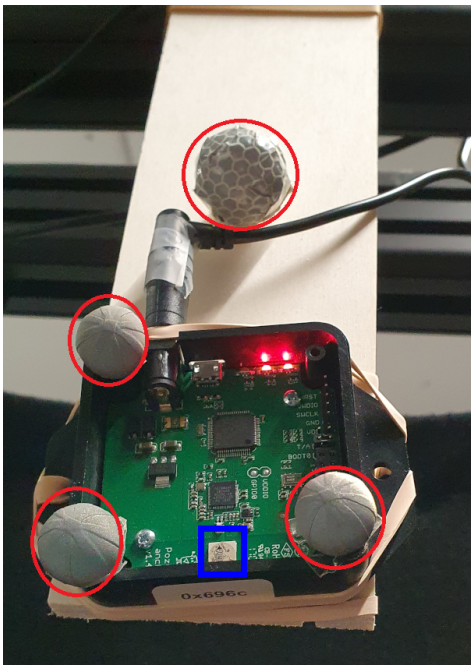

**Figure 5.2:** An example of Optitrack markers (for reference purposes) attached to an ANC. Each ANC was provided with an unique marker configuration for automatic recognition by Motive (Optitrack software).

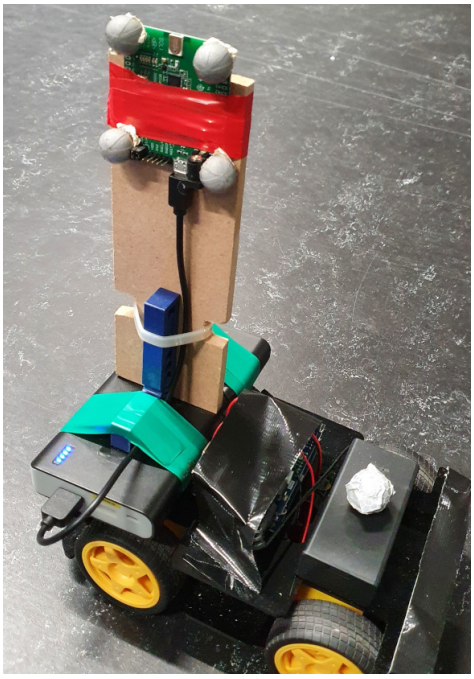

**Figure 5.3:** The RC-car with the Optitrack markers (for reference purposes). Five markers were used to create unique marker configuration for automatic recognition by Motive (Optitrack software).

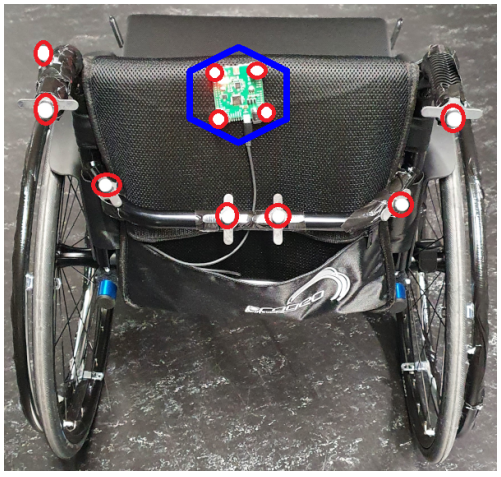

**Figure 5.4:** The wheelchair used in the measurements.. The wheelchair has 7 Optitrack markers, illustrates with red circles, and a UWB TAG illustrated with a blue hexagon, attached to the backseat of the wheelchair. This is the *Non-Line-Of-Sight* (NLoS) setup as a wheelchair user blocks the UWB signal partially.

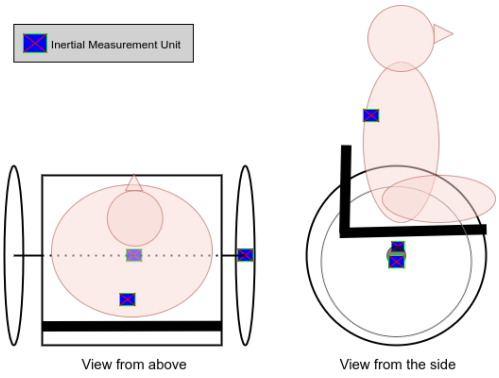


**Figure 5.5:** Schematic of the placements of IMUs in the WMPM system.

## 5.4 Post processing

All datasets were converted and synced with Matlab R2020a. Every measurement was visually checked for integrity with Matlab. The Optitrack measurements had on average 10 % of missing markers. This percentage is acceptable for evaluation purposes. The missing markers are not filtered or 'filled' in the sensor fusion algorithm and ignored in the calculations of the performance evaluation.

# Chapter 6

# Evaluation

This chapter covers the evaluation of the localization algorithms (chapter 3) and the sensor fusion solution (chapter 4).

## 6.1 Simulations

The performance of the localization algorithms is initially checked with simulations. Simulations give more freedom in an analysis compared to measurements. For example, the number of UWB ANCs in the measurements was limited to four, but simulations do not have these limitations. To evaluate the effects of the number of ANCs, five noiseless datasets with 3 to 7 ANCs were created, each with more than 30000 samples. Such a noiseless dataset was used as a validity check for each algorithm. A localization error based on this clean dataset would suggest an error in the algorithm or otherwise a reason to discard it. All other simulations include the noise model described in section 3.5.

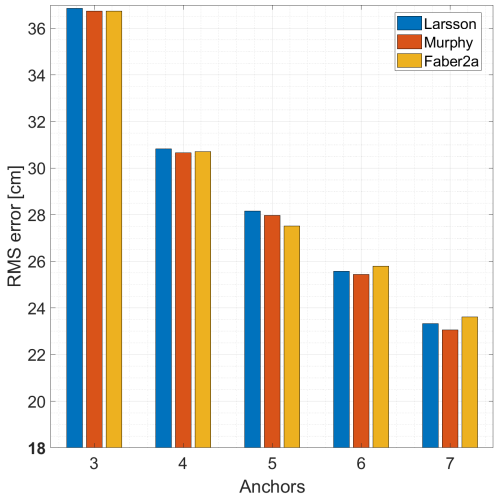


**Figure 6.1:** The cumulative *Root Mean Square Error* (RMSE) values of the localization algorithms related to the number of ANCs. Please note the starting value of the y-axis.

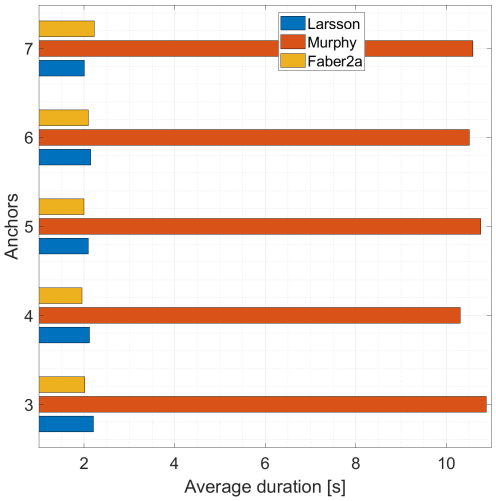


**Figure 6.2:** The cumulative duration of all simulations, related to the number of ANCs.

Figure 6.1 shows the cumulative localization error related to the number of ANCs. It can be observed that the differences between the algorithms are small. To check the resemblance of the Larsson and Faber algorithm with Murphy the Intra-Class-

Correlation (ICC) was calculated. All combinations gave an ICC of more than 0.98 ($\alpha = 0.01$). It can be concluded that there are no localization differences based on the simulations.

Figure 6.2 shows the execution time of the localization algorithms that was measured with Matlab. There is in general no observed difference in execution time related to the number of ANCs. The Faber is 5.2 times faster than the previously implemented method of Murphy. Larsson is 5 times faster than Murphy. Both could be a good alternative to Murphy, but that choice also depends on the measurement results.

## 6.2 Measurements

Different static and dynamic measurements were done as described in chapter 5. This section covers the following type of measurements:

- Static LoS with Murphy, Larsson and Faber
- Dynamic LoS with Murphy, Larsson and Faber
- Dynamic NLoS with Murphy, Larsson and Faber
- Static LoS with a proprietary Pozyx algorithm (a black box)
- Dynamic LoS with a proprietary Pozyx algorithm

### 6.2.1 Static LoS

The TAG was placed in the approximate center of the ANC constellation on the ground and did not move. These static ranging measurements served as localization input and the localtion is compared to the groundtruth location. The differences between UWB location and groundtruth are visualized in figure 6.3.

For visualization of the error a violin-plot is used. This is a box-plot where the box is replaced by a density distribution. The black line represents the mean ($\mu$), the red dot represents the median, the gray rectangle illustrates the first and third quartile. In this document it can be used to check, for instance, what level of error occurs most.

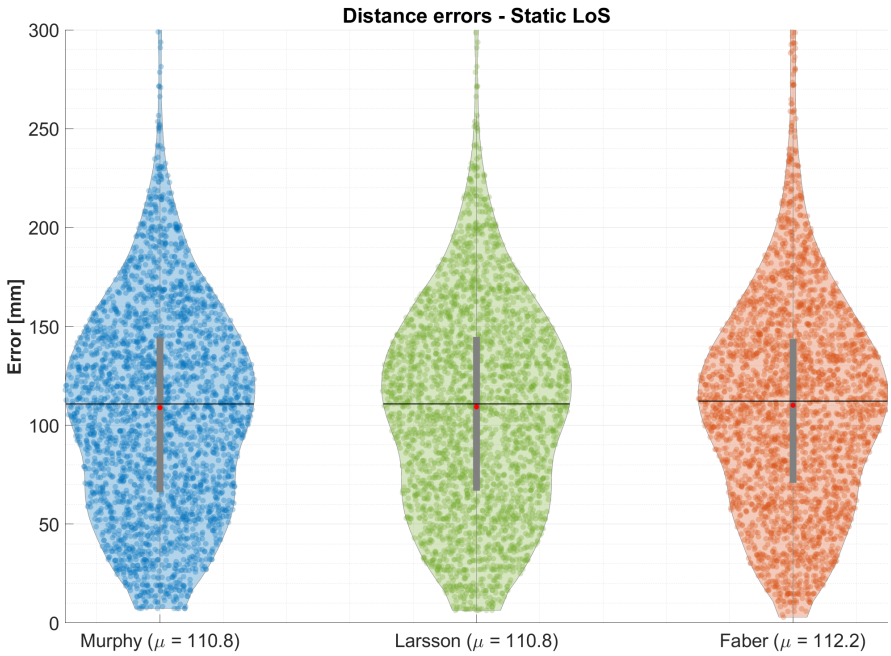


**Figure 6.3:** A violin plot of UWB errors. Average update rate 7.5 Hz.

The distributions in figure 6.3 are not Gaussian. In general, the three algorithms perform similarly where Faber has a slightly higher average error. In the dynamic measurements the TAG is moving and there is more diversity in the ranges, which tends to give a normal distribution.

### 6.2.2 Dynamic LoS

Figure 6.4 show the results of the dynamic LoS measurements. The average velocity of the TAG was $6\,\mathrm{m\,s^{-1}}$. The average error in the dynamic measurements is, remarkably, slightly lower than in the static measurements. This can be explained by the fact that the TAG in the static case was approximately in the center of the ANCs. If a certain TAG-ANC combination performs slightly worse, then this will result in a larger error. The ranging result of the closest ANC will probably determine the location the most. Moreover, the Faber algorithm has a larger average error due to more outliers. These measurements show that Larsson has the best practical localization accuracy in dynamic situations, which is the case in wheelchair situations.

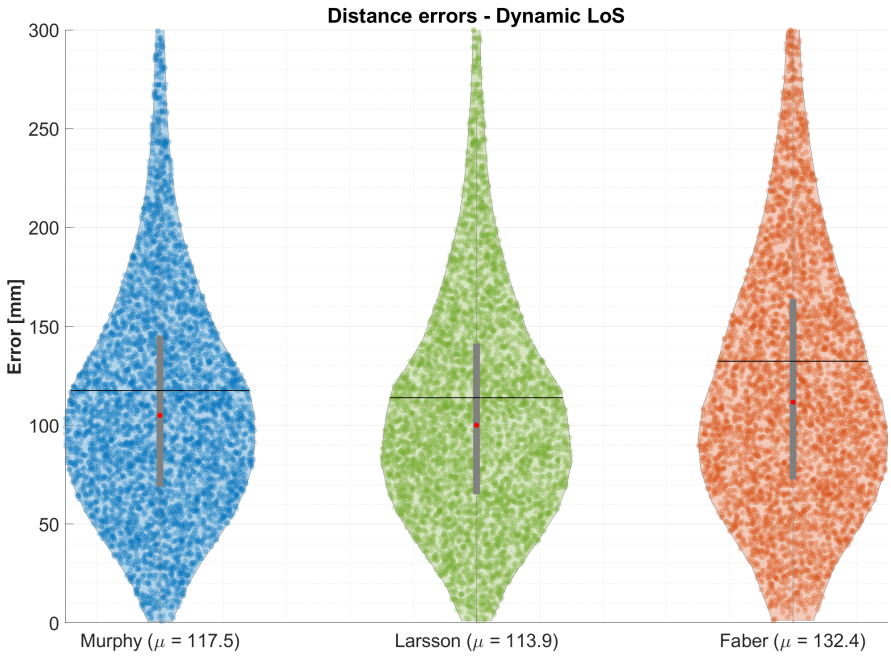


**Figure 6.4:** A violin plot of UWB measurements (reference Optitrack). Average update rate 7.5 Hz. For each localization algorithm the mean ($\mu$) error is displaced at the rightside of the label.

### 6.2.3 Pozyx proprietary localization LoS

The Pozyx system has a proprietary algorithm to perform localization for its users. Comparing the results in figure 6.3 and figure 6.4 with figure 6.5 shows that the accuracy of the Pozyx proprietary localization algorithm (PLA) is slightly better than the Larsson algorithm. In this case, the PLA performs on average in the dynamic case better by 7.7 mm RMSE. This is explained by an Pozyx update rate that is 2.3 times higher and an lower average TAG velocity.

### 6.2.4 Dynamic NLoS

The Dynamic NLoS measurements, with wheelchair and person are shown in figure 6.6. Similar to the dynamic LoS Larsson has the highest accuracy, but the plots show more outliers which is explained by the velocity of the TAG.

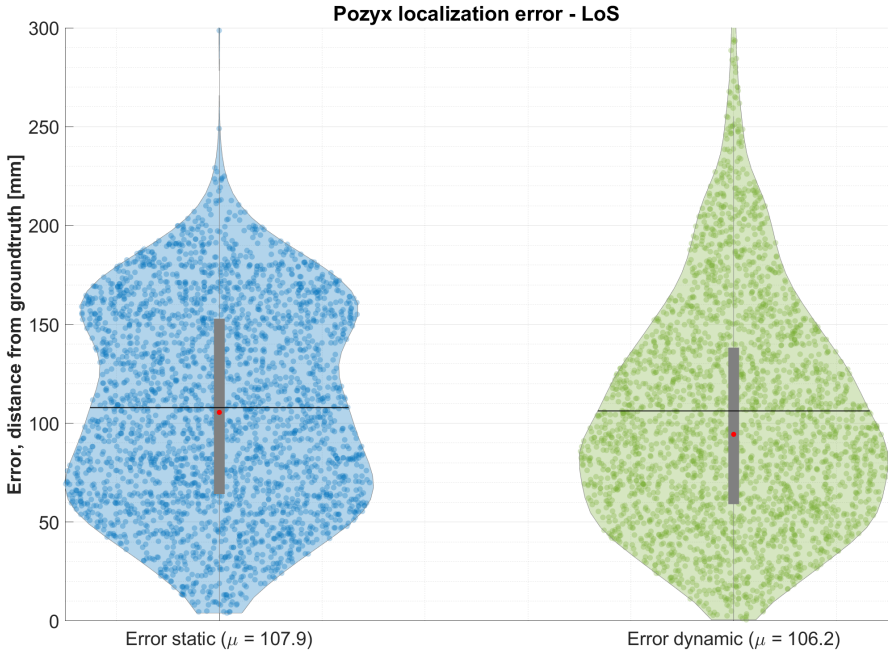


**Figure 6.5:** The violin plots of the proprietary Pozyx algorithm in a static and dynamic LoS situation. Average update rate 16.8 Hz. The average velocity of the TAG was $3\,\mathrm{m\,s^{-1}}$.

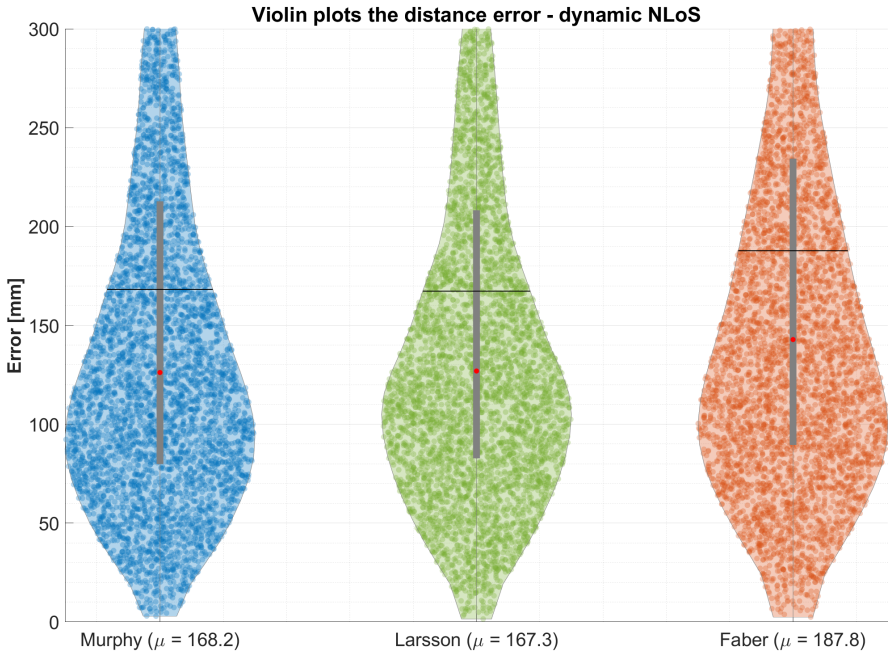


**Figure 6.6:** The violin plots of the dynamic NLoS measurements. The average update rate was 7.5 Hz and the average velocity of the TAG was $6.2\,\mathrm{m\,s^{-1}}$.

### 6.2.5 Conclusion

The simulation results show that the three localization algorithms are similar in performance. Especially the dynamic LoS measurements show some nuance in the differences. For instance, Faber has a reduced performance which makes it less suitable. The Pozyx proprietary localization performs better than Larsson, which is explained by the differences in update rate and TAG velocity. This requires more investigation

to compare their differences. Because Faber and Larsson are approximately 5 times faster than Murphy and Larsson has the best accuracy, Larsson is the algorithm of choice in the Sensor fusion.

## 6.3 Sensor fusion

The results of the UKF chapter are shown in table 6.1. The first column shows the UWB RMSE and gives an indication on the precision of UWB Larsson localization off the bat. The second column shows the RMSE when IMU and UWB is combined. By implementing the RTS-smoother the RMSE further reduces to an average RMSE of 123.9 mm. On average the UKF RTS implementation gives a 43.8 % reduction in RMSE compared to UWB. In figure 6.7 this is visualized by the 2D-coordinates.

| # | UWB RMSE | UKF RMSE | UKF RTS RMSE | % UKF | % UKF RTS |
|---|---|---|---|---|---|
| 1 | 194.8 | 146.0 | 115.3 | −25.1 | −40.8 |
| 2 | 248.8 | 155.5 | 116.2 | −37.5 | −53.3 |
| 3 | 229.6 | 185.1 | 130.7 | −19.4 | −43.1 |
| 4 | 239.2 | 167.1 | 128.5 | −30.1 | −46.3 |
| 5 | 199.4 | 169.0 | 128.9 | −15.3 | −35.4 |

**Table 6.1:** Measurement (#) results expressed in RMSE (in mm) are based on ground truth reference. The percentual error change has as reference the UWB RMSE and is indicated by %. A negative change indicates a reduction

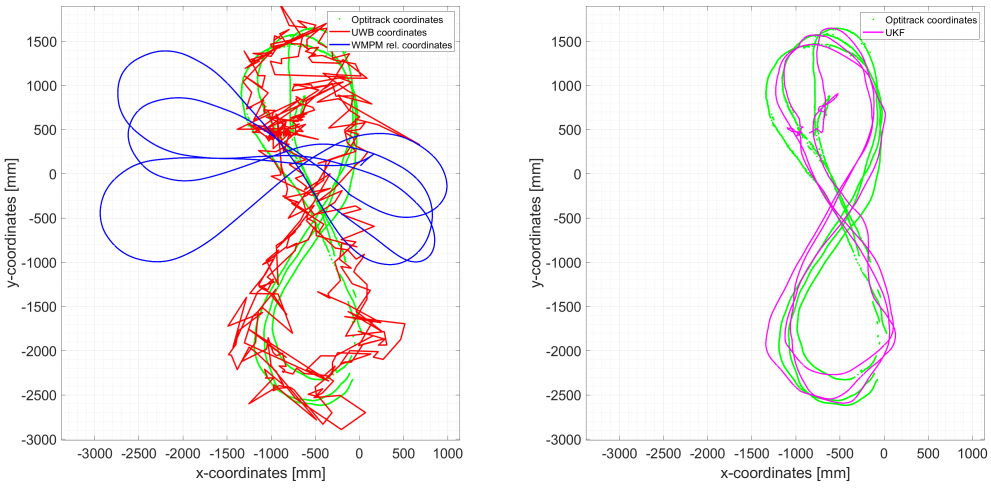


**Figure 6.7: Left:** The groundtruth (green) with the input data for sensor fusion. **Right:** The groundtruth with the UKF (magenta) result.

### 6.3.1 Measurement limitations

The UWB ranging measurements had a relatively low update rate of 7.5 Hz. This was not observed during initial tests in a smaller room of 2 m by 3 m, where the setup had an update rate of over 15 Hz. The manufacturer suggested that a dedicated telemetry module (e.g. a wifi modules) per ANC would resolve this. There were no indications during the initial test that a larger room, as used in the measurements, would give this reduction.

The reduced update rate also reduces the accuracy of localization. When TWR is used each TAG and ANC range is registered in sequence. Consecutive measured ranges of a moving TAG will give an increased localization error. This inevitable inaccuracy can be alleviated, in a future setting, by increasing the update rate.

# Chapter 7

# Conclusion and Future work

## 7.1 Conclusion

Measuring the performance of an athlete is important for coaches to evaluate the game they have played. A recently developed IMU measurement system, the WMPM, tracks the kinematics of wheelchair athletes. This odometry-based system, gives coaches offline kinematic wheelchair feedback and the relative location of an athlete. But game analysis requires that the absolute location of a wheelchair athlete is known. UWB is a good candidate to extend the WMPM with absolute location. However, it is unclear if this would give the desired precision.

The WMPM system would ideally give a coach, in the future, real-time game information. This requires that the localization algorithm is as fast as possible. Previously, a master thesis by Pathi [28] at the TU Delft describes a sports related UWB implementation. Pathi used the localization algorithm described by Murphy et. al. [24]. This work started with this Murphy localization algorithm. Recent work by Larsson et. al. [16] was found that could potentially provide faster localization. Additionally, a collaboration with H. Faber (The Hague University of Applied Sciences) started which resulted in the Faber localization algorithm. The comparison of Murphy, Larsson and Faber was done in a set of simulations and showed that Larsson and Faber were approximately 5 times faster than Murphy. Moreover, the accuracy of the algorithms was shown to be the same (ICC of 0.98 or higher, $\alpha = 0.01$). The simulations were validated with measurements, combining an UWB system by Pozyx, the WMPM and a IR-camera system by Optitrack. The Pozyx UWB system came with a proprietary localization algorithm, which was compared to Murphy, Larsson and Faber. The measurements show that Pozyx algorithm has a better performance of on average 7.7 mm RMSE. However, the Pozyx proprietary algorithm had a higher update rate of 16.8 Hz compared to UWB ranging at 7.5 Hz and had a lower TAG velocity. This requires a better comparison, in future work, where similar TAG velocity and update rates are maintained. A higher update rate will generally give a better TWR localization accuracy. It is concluded, that Larsson is a good alternative for Murphy and the proprietary Pozyx algorithm.

This project aims to improve wheelchair pose tracking by combining UWB and the WMPM which requires sensor fusion. Different sensor fusion methods were investigated and simulated. Due to the non-linear nature of the measurement data and the movement model, it was decided to use the Unscented Kalman Filter. Due to the multi-rate nature of the systems (UWB and WMPM) the UKF showed a poor precision and a localization offset. A Rauch-Tung-Striebel (RTS) smoother was implemented to improve this. After a tuning process, an average localization improvement,

compared to UWB, was obtained of 43.8 %. This work provides a basis for future wheelchair pose tracking development and shows that UWB could be a good addition to the WMPM.

## 7.2 Future work

The update rate of the UWB ranging solution in this work was undesirably low. The minimum update rate should be at least 15 Hz [18]. It is suggested, after a conversation with Pozyx, that a higher update rate in that vicinity is achievable if each ANC would get its own telemetry module (Wi-Fi or Bluetooth). The UKF localization performance could furthermore be improved by enabling the wheelchair frame accelerometer, which was disabled due to bandwidth limitations. This could be improved in the next version of the WMPM that includes UWB. Furthermore, this future version should enable the accelerometer of the wheelchair frame IMU. The accelerometer data will provide extra measurement information for the sensor fusion, eliminating the tracking of one 'hidden' state variable.

Due to the achieved absolute pose tracking in this project, there is another way to deal with NLoS. The orientation of a wheelchair could be used to determine which ANC must give ranging information based on NLoS. This specific NLoS based ranging information could be removed from the real-time localization algorithm (i.e. Larsson) which could provide better results.

The measurements in this project included only one type of NLoS, due to one wheelchair and one person. But in a sport setting up to ten athletes could be on the court and it is unclear what the localization performance would be with this number of athletes. To minimize the effects of NLoS the ANCs should be placed high at 2.5 m or more, alongside the court. This way NLoS due the wheelchair athletes is minimized[1]. A dynamic test with four wheelchair users would be an appropriate start.

In other related work, the PF is implemented to improve UWB localization [19]. This is due to its inherent ability of non-linear estimation and the handling of multi-modality (i.e. tracking multiple athletes). The biggest disadvantage of the PF though, is that it requires much more computational power, which makes real-time tracking unfeasible. However, it could reduce the setup complexity by reducing the number of ANCs. For example, with a strategic placement of two ANCs, assuming 2D tracking, each range between a TAG and two ANCs, would give two circles. A solution that knows the ANC locations, relative to the court, could use logic to ignore the intersection of these two circles (i.e. the TAG location) outside of the court. This means that localization could, theoretically, be obtained by two ANCs, reducing the setup complexity. Sensor fusion would again be needed to obtain improved precision.

[1] Compared to an ANCs on the floor of the court that would *always* lead to NLoS.

# Bibliography


[1] Website: Wikipedia, Quantified self, (accessed: 13.07.2020).

[2] Website: Quantified self; self knowledge through numbers, (accessed: 13.07.2020).

[3] Website: Google Scholar, UWB and Localization, (accessed: 13.07.2020).

[4] Bardia Alavi and Kaveh Pahlavan. Modeling of the toa-based distance measurement error using uwb indoor radio measurements. *IEEE communications letters*, 10(4):275–277, 2006.

[5] Valentina Camomilla, Elena Bergamini, Silvia Fantozzi, and Giuseppe Vannozzi. Trends supporting the in-field use of wearable inertial sensors for sport performance evaluation: A systematic review. *Sensors*, 18(3):873, 2018.

[6] Federico Castanedo. A review of data fusion techniques. *The scientific world journal*, 2013, 2013.

[7] Pablo Corbalán, Gian Pietro Picco, and Sameera Palipana. Chorus: Uwb concurrent transmissions for gps-like passive localization of countless targets. In *Proceedings of the 18th International Conference on Information Processing in Sensor Networks*, pages 133–144. ACM, 2019.

[8] AMH De Witte, Rienk MA van der Slikke, MAM Berger, Marco JM Hoozemans, HEJ Veeger, and LHV Van Der Woude. Effects of seat height, wheelchair mass and additional grip on a field-based wheelchair basketball mobility performance test. *Technology and Disability*, 32(2):93–102, 2020.

[9] Bruno Figueira, Bruno Gonçalves, Hugo Folgado, Nerijus Masiulis, Julio Calleja-González, and Jaime Sampaio. Accuracy of a basketball indoor tracking system based on standard bluetooth low energy channels (nbn23®). *Sensors*, 18(6):1940, 2018.

[10] Antoine Fleureau, Mathieu Lacome, Martin Buchheit, Antoine Couturier, and Giuseppe Rabita. Validity of an ultra-wideband local positioning system to assess specific movements in handball. *Biology of Sport*, 37(4):351, 2020.

[11] Bernhard Groβwindhager, Michael Stocker, Michael Rath, Carlo Alberto Boano, and Kay Römer. SnapLoc: an ultra-fast UWB-based indoor localization system for an unlimited number of tags. In *2019 18th ACM/IEEE International Conference on Information Processing in Sensor Networks (IPSN)*, pages 61–72. IEEE, 2019.

[12] Bernhard Großwindhager, Michael Rath, Josef Kulmer, Mustafa S Bakr, Carlo Alberto Boano, Klaus Witrisal, and Kay Römer. Salma: Uwb-based single-anchor localization system using multipath assistance. In *Proceedings of the 16th ACM Conference on Embedded Networked Sensor Systems*, pages 132–144. ACM, 2018.

[13] Simon J Julier and Jeffrey K Uhlmann. New extension of the kalman filter to nonlinear systems. In *Signal processing, sensor fusion, and target recognition VI*, volume 3068, pages 182–193. International Society for Optics and Photonics, 1997.

[14] Simon J Julier and Jeffrey K Uhlmann. Unscented filtering and nonlinear estimation. *Proceedings of the IEEE*, 92(3):401–422, 2004.

[15] Regina Kaune. Accuracy studies for tdoa and toa localization. In *2012 15th International Conference on Information Fusion*, pages 408–415. IEEE, 2012.

[16] Martin Larsson, Viktor Larsson, Kalle Astrom, and Magnus Oskarsson. Optimal Trilateration Is an Eigenvalue Problem. In *ICASSP 2019-2019 IEEE International Conference on Acoustics, Speech and Signal Processing (ICASSP)*, pages 5586–5590. IEEE, 2019.

[17] Joo-Ho Lee and Hideki Hashimoto. Intelligent space—concept and contents. *Advanced Robotics*, 16(3):265–280, 2002.

[18] Roland Leser, Arnold Baca, and Georg Ogris. Local positioning systems in (game) sports. *Sensors*, 11(10):9778–9797, 2011.

[19] Roland Leser, Armin Schleindlhuber, Keith Lyons, and Arnold Baca. Accuracy of an uwb-based position tracking system used for time-motion analyses in game sports. *European journal of sport science*, 14(7):635–642, 2014.

[20] Swen Leugner, Mathias Pelka, and Horst Hellbrück. Comparison of wired and wireless synchronization with clock drift compensation suited for u-tdoa localization. In *2016 13th Workshop on Positioning, Navigation and Communications (WPNC)*, pages 1–4. IEEE, 2016.

[21] A Martinelli, M Dolfi, S Morosi, L Mucchi, M Paoli, and A Agili. Ultra-wide band positioning in sport: How the relative height between the transmitting and the receiving antenna affects the system performance. *International Journal of Wireless Information Networks*, pages 1–12, 2019.

[22] Rainer Mautz. Indoor positioning technologies. 2012.

[23] James R Morrow Jr, Dale Mood, James Disch, and Minsoo Kang. *Measurement and Evaluation in Human Performance, 5E*. Human Kinetics, 2015.

[24] William S Murphy. Determination of a position using approximate distances and trilateration. *Colorado School of Mines*, 2007.

[25] Daniel Neuhold, Christian Bettstetter, and Andreas F Molisch. Hipr: High-precision uwb ranging for sensor networks. In *Proceedings of the 22nd International ACM Conference on Modeling, Analysis and Simulation of Wireless and Mobile Systems*, pages 103–107, 2019.

[26] Ian Oppermann, Matti Hämäläinen, and Jari Iinatti. *UWB: theory and applications*. John Wiley & Sons, 2005.

[27] Timothy Otim, Alfonso Bahillo, Luis Enrique Díez, Peio Lopez-Iturri, and Francisco Falcone. Impact of body wearable sensor positions on uwb ranging. *IEEE Sensors Journal*, 2019.

[28] Vinay Pathi Balaji. THESIS Virtual Referee: A system to identify off-sides in Football. 2019.

[29] Bertrand Perrat, Martin J Smith, Barry S Mason, James M Rhodes, and Vicky L Goosey-Tolfrey. Quality assessment of an ultra-wide band positioning system for indoor wheelchair court sports. *Proceedings of the Institution of Mechanical Engineers, Part P: Journal of Sports Engineering and Technology*, 229(2):81–91, 2015.

[30] Jitendra R Raol. *Multi-sensor data fusion with MATLAB*. CRC press, 2009.

[31] Herbert E Rauch, F Tung, and Charlotte T Striebel. Maximum likelihood estimates of linear dynamic systems. *AIAA journal*, 3(8):1445–1450, 1965.

[32] Markel Rico-González, José Pino-Ortega, Fabio Y Nakamura, Felipe Arruda Moura, Daniel Rojas-Valverde, and Asier Los Arcos. Past, present, and future of the technological tracking methods to assess tactical variables in team sports: A systematic review. *Proceedings of the Institution of Mechanical Engineers, Part P: Journal of Sports Engineering and Technology*, 234(4):281–290, 2020.

[33] Matteo Ridolfi, Stef Vandermeeren, Jense Defraye, Heidi Steendam, Joeri Gerlo, Dirk De Clercq, Jeroen Hoebeke, and Eli De Poorter. Experimental evaluation of uwb indoor positioning for sport postures. *Sensors*, 18(1):168, 2018.

[34] Thomas Rietveld, Riemer JK Vegter, Rienk MA van der Slikke, Aldo E Hoekstra, Lucas HV van der Woude, and Sonja de Groot. Wheelchair mobility performance of elite wheelchair tennis players during four field tests: Inter-trial reliability and construct validity. *PloS one*, 14(6):e0217514, 2019.

[35] Margreet Riphagen, Marco van Hout, D Kritjnen, and Gijs Gootjes. Learning tomorrow: visualising student and staff's daily activities and reflect on it. *URL: http://medialabamsterdam. com/wp-content/uploads/2013/11/ICERIE2013_ Paper_M_Riphagen_AUAS. pdf (visited on 07/27/2016)*, 2013.

[36] Antonio Ramón Jiménez Ruiz and Fernando Seco Granja. Comparing ubisense, bespoon, and decawave uwb location systems: Indoor performance analysis. *IEEE Transactions on instrumentation and Measurement*, 66(8):2106–2117, 2017.

[37] J Sachs, M Helbig, R Herrmann, M Kmec, and K Schilling. On the range precision of uwb radar sensors. In *11-th International Radar Symposium*, pages 1–4. IEEE, 2010.

[38] Thuraiappah Sathyan, Mark Hedley, and Mahendra Mallick. An analysis of the error characteristics of two time of arrival localization techniques. In *2010 13th International Conference on Information Fusion*, pages 1–7. IEEE, 2010.

[39] Juri Sidorenkoab, Volker Schatza, Norbert Scherer-Negenborna, Michael Arensa, and Urs Hugentobler. Decawave UWB clock drift correction and powerself-calibration. *arXiv preprint arXiv:1902.11085*, 2019.

[40] James D Taylor. *Introduction to ultra-wideband radar systems*. CRC press, 1994.

[41] Myo Min Thein and Son Nguyen. Thesis comparing the accuracy of bluetooth low energy and uwb technology for in-room positioning. 2019.

[42] Ciza Thomas. *Sensor fusion and its applications*. BoD–Books on Demand, 2010.

[43] Rudolph Van Der Merwe et al. *Sigma-point Kalman filters for probabilistic inference in dynamic state-space models*. PhD thesis, OGI School of Science & Engineering at OHSU, 2004.

[44] Rienk van der Slikke, Monique AM Berger, Daan JJ Bregman, and Dirkjan HEJ Veeger. Wearable wheelchair mobility performance measurement in basketball, rugby, and tennis: Lessons for classification and training. *Sensors*, 20(12):3518, 2020.

[45] Rienk MA van der Slikke, Daan JJ Bregman, Monique AM Berger, Annemarie MH De Witte, et al. The future of classification in wheelchair sports: can data science and technological advancement offer an alternative point of view? *International journal of sports physiology and performance*, 13(6):742–749, 2018.

[46] RMA van der Slikke. *Out of the lab, onto the court: Wheelchair Mobility Performance quantified*. PhD thesis, Delft University of Technology, 2018.

[47] RMA Van Der Slikke, MAM Berger, DJJ Bregman, AH Lagerberg, and HEJ Veeger. Opportunities for measuring wheelchair kinematics in match settings; reliability of a three inertial sensor configuration. *Journal of Biomechanics*, 48(12):3398–3405, 2015.

[48] RMA Van der Slikke, MAM Berger, DJJ Bregman, and HEJ Veeger. Wheel skid correction is a prerequisite to reliably measure wheelchair sports kinematics based on inertial sensors. *Procedia Engineering*, 112:207–212, 2015.

[49] RMA Van der Slikke, MAM Berger, DJJ Bregman, and HEJ Veeger. From big data to rich data: the key features of athlete wheelchair mobility performance. *Journal of biomechanics*, 49(14):3340–3346, 2016.

[50] RMA van der Slikke, Barry S Mason, MAM Berger, and Victoria L Goosey-Tolfrey. Speed profiles in wheelchair court sports; comparison of two methods for measuring wheelchair mobility performance. *Journal of biomechanics*, 65:221–225, 2017.

[51] Rienk MA van der Slikkea, Annemarie MH de Wittea, Daan JJ Bergera, Dirk Jan HEJ Veegerb, and Johanna Westerdijkplein. Wheelchair mobility performance enhancement by changing wheelchair properties; what is the effect of grip, seat height and mass? submission type. *ijspp*, 2017(0641):0641, 2018.

[52] Eric A Wan and Rudolph Van Der Merwe. The unscented kalman filter for nonlinear estimation. In *Proceedings of the IEEE 2000 Adaptive Systems for Signal Processing, Communications, and Control Symposium (Cat. No. 00EX373)*, pages 153–158. Ieee, 2000.

[53] Eric A Wan, Rudolph Van Der Merwe, and Simon Haykin. The unscented kalman filter. *Kalman filtering and neural networks*, 5(2007):221–280, 2001.

[54] Jun Xu, Maode Ma, and Choi Look Law. Theoretical lower bound for uwb tdoa positioning. In *IEEE GLOBECOM 2007-IEEE Global Telecommunications Conference*, pages 4101–4105. IEEE, 2007.

# Appendices

# Appendix A

# Acronyms

**ANC** Anchor (*A static UWB transceiver with a know location. Also known as: beacon. The tag and anchor transmit UWB signals to determine their respective distance. Anchors are sometimes called* ***sensors***), p. 4

**AoA** Angle-of-Arrival (*By using certain antenna configuration the angle of a messag can be determined from which triangulation or multiangulation can be applied*), p. 53

**BW** Bandwidth (*A range of frequencies.*), p. 21

**CRLB** Cramer Rao Lower Bound (*A lower bound for the variance of 'unbiased estimators'. An estimator that achieves this theoretical lower bound is most efficient.*), p. 10

**DWM1000** DecaWave D1000 Radio Chip (*The chip that is thought to have stimulated the increase in popularity of UWB. source.*), p. 2

**EKF** Extended Kalman Filter (*See: Kalman Filter and Unscented Kalman Filter.*), p. 9

**GPS** Global Positioning System (*A system with accurately synchronized sattelites that send their coordinates and time-of-transmission. From this the time-of-arrival can be calculated from which the true-range (distance) can be determined.*), p. 7

**ICC** Intra class correlation (*A descriptive statistic a measure which describes how strongly units of the same group are similar.* ), p. 39

**IEEE 802.15.4** IEEE Ultra Wide band (*The ranging standard is defined in IEEE 802.15.4a link. It specifies the physical layer and media access control for Low-Rate wireless personal area networks.*), p. 4

**IMU** Inertial Measurement Unit (*In this document it is referred to as a device with a 3DoF Accelerometer, 3DoF Gyroscope and a 3Dof Magnetometer.*), p. iii

**KF** Kalman Filter (*A filter that uses measurements that contain noise and a model of the object that is 'filtered' which often produces better results than one single measurement. The Kalman Filter is less suited for non-linear situations (see: Extended Kalman Filter and Unscented Kalman filter).*), p. 22

**LoS** Line-Of-Sight, p. 4

**MOCAP** Marker Based Motion Capture System, p. 2

**MPC** multipath components (*UWB is relatively resilient against multipath components compared to narrowband because it transmits short pulses over a large bandwidth.*), p. 11

**NLoS** Non-Line-Of-Sight, p. iii

**PF** Particle Filter, p. 9

**PLL** Phase Locked Loop (*A control circuit that tracks the difference between the input and output phase (locking) which can be used for clock synchronization.*), p. 12

**RMSE** Root Mean Square Error (*Generally used to measure the error of prediction. It is a measure of accuracy. It increases with the variance of the frequency distribution of the error.* ), p. iii

**TAG** Tag (*The UWB transceiver that is attached to an object that needs to be localised. Also know as: Node.*), p. 2

**TDoA** Time Difference of Arrival (*The difference of arrival times of a packet from synchronized senders (e.g. anchors). This method will be used if there is no synchronization between a sender and a receiver (anchor and tag).* ), p. 5

**ToA** Time-of-Arrival (*The timestamp at which a message has been received. Please note, that this timestamp has the time-reference of the receiver (i.e. TAG and ANCHOR are not necessarily synchronized which means they each has their own time reference).*), p. 5

**ToF** Time-of-Flight (*The time taken by a particle or a wave to travel through a medium (e.g. from ANCHOR to TAG). This information can be used to derive the distance. For ToF synchronized TAGs and ANCHORS are needed.*), p. 5

**TWR** Two Way Ranging (*Ranging between two transceivers when they are not synchronized. This method applies synchronization by sending multiple messages.*), p. 5

**UKF** Unscented Kalman Filter (*See: Kalman Filter and Extended Kalman Filter.*), p. iii

**UWB** Ultra-wideband (*A radio technology which can be used for short-range, high-bandwidth and low energy communications but also for* ***ranging****.*), p. iii

**WMPM** Wheelchair Mobility Performance Monitor (*A method to measure wheelchair mobility performance.*), p. iii

# Appendix B

# Miscellaneous

## B.1 Position versus location

In this project UWB is investigated with regards to producing coordinates. What should the process of obtaining *coordinates* be called? There are two possibilities: *localization* and *positioning*. Positioning often includes *orientation*. If you rotate a coffee mock that is placed on a surface, the location is the same but its position is changed. Or, it's location is the same but the orientation is changed. [1] UWB only provides location, thus localization is the more descriptive term.

## B.2 Accuracy and precision

The definitions accuracy and precision are easily confused. ***Accuracy*** is the term that describes the deviation between a measured value $\widehat{d}$ and the true value $d$. A low deviation means a high accuracy. The deviation or error $\epsilon$ should be as small as possible and can be denoted as:

$$\epsilon_i = \widehat{d}_i - d \tag{B.1}$$

Here $i$ denotes a single measurement. Accuracy can then be defined, when $n$ is sufficiently high, as the average error:

$$\bar{\epsilon} = \frac{1}{n}\sum_{i=1}^{n}\epsilon_i \tag{B.2}$$

***Precision*** is defined as the inverse [2] of the variability of $\widehat{d}$. E.g. if all the $\widehat{d}_i$ are close to each other (i.e. low variability) there is a *high* precision. Denoted:

$$\sigma_\epsilon^2 = \frac{1}{n-1}\sum_{i=1}^{n}(\epsilon_i - \bar{\epsilon})^2 \tag{B.3}$$

[1] UWB does not give orientation.

[2] Note that no inversion is shown. It is assumed the reader knows that a low variability means a high precision in this context.

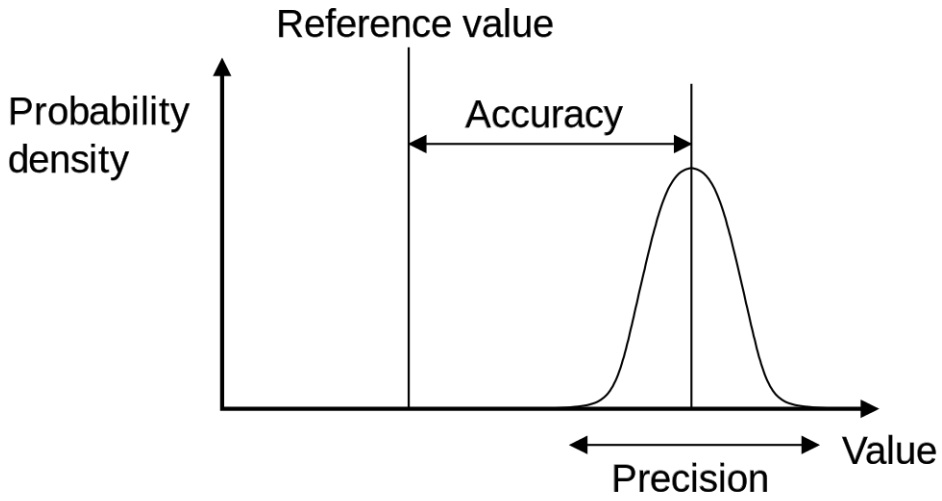


**Figure B.1:** Visualisation of accuracy versus precision. Source Wikipedia.

## B.3 Error function

To determine the performance of an algorithm an error function needs to be defined. In this section some options are covered.

The investigated trilateration algorithms (e.g. Murphy, Larsson, etc.) are initially simulated. To simulate an localization algorithm a setup of $K$ ANCs and a TAG is created, see figure 3.1. A measurement consists of a trajectory of the TAG in time which consists of $N$ measurements. The *true* distances $d_i$ in that situation are known. In the simulations to every *true* distance $d_i$ also some noise is added ($\widetilde{d_i}$).

A trilateration algorithm outputs the *calculated* position $\mathbf{x}^*$. In a real scenario (by doing actual ranging measurements) the *measured* distances $\widetilde{d_i}$ are known. [3].

### B.3.1 The error function in simulation

In simulation the *true* position of a TAG is known. This gives 2 options to express an error function, namely based on the position and based on distances.

### B.3.2 Positions

Figure 3.1 illustrates the parameters in trilateration. The true positions of the ANCs and TAG are known. Then their respective distances ($d_i$) can be calculated which are also polluted with some noise ($\widetilde{d_i}$). Those distances are the input for the trilateration algorithm which outputs the $\widetilde{\mathbf{x}^*}$ which consists of the $(\widetilde{x^*}, \widetilde{y^*})$ coordinates. The distance $d_p$ between $\mathbf{x}$ and $\widetilde{\mathbf{x}^*}$ can be calculated and used in an error function:

$$e_{tpos} = \sqrt{\frac{\sum_{j=0}^{N} ||\mathbf{x}_j - \widetilde{\mathbf{x}_j^*}||^2}{N}} = \sqrt{\frac{\sum_{j=0}^{N} d_{p\_j}}{N}} \tag{B.4}$$

[3] Please note that no difference is made between measured distances and *true* distances with added noise.

### B.3.3 Distances

Instead of using the position an error function $e_{tdis}$ can be conceived. In this error function the distances $\widetilde{d_i^*}$ are calculated based on $\widetilde{d_i}$. This function is better comparable to the error function used in a practical scenario as described in section B.3.4.

$$e_{tdis} = \sqrt{\frac{\sum_{i=0}^{K}\sum_{j=0}^{N}\left(d_{ij} - \widetilde{d_{ij}^*}\right)^2}{K \cdot N}} \tag{B.5}$$

### B.3.4 The practical error function

In a practical situation the *true* location of a TAG is not known. A trilateration algorithm provides a calculated position based on measurements $\widetilde{d_{ij}}$. Because the absolute location of the ANCs is known, the calculated location $\widetilde{\mathbf{x}^*}$ can again be used to determine the distance between $\widetilde{\mathbf{x}^*}$ and the anchors $\mathbf{a}_i$ with $\widetilde{d_{ij}^*} = ||\widetilde{\mathbf{x}^*} - \mathbf{a}_i||$.

$$e_{cdis} = \sqrt{\frac{\sum_{i=0}^{K}\sum_{j=0}^{N}\left(\widetilde{d_{ij}} - \widetilde{d_{ij}^*}\right)^2}{K \cdot N}} \tag{B.6}$$

### B.3.5 Error function choice

It is clear that equation B.6 will be used to express the performance of the localization system as the *true* distances are not known. For simulation purposes equation B.5 is most comparable and thus the best option to use.

## B.4 UKF mathematical model

This section briefly covers the mathematics behind the UKF. It is assumed that the reader knows the basic steps from the KF and it is furthermore related to figure 4.6.

$$\boldsymbol{\mathcal{Y}} = \mathbf{F}(\boldsymbol{\chi}) \tag{B.7}$$

As seen in figure 4.6 the weights $w_i^m$ and $w_i^c$ serve as input to create each $i$-th sigma point. Then the mean state vector $\hat{\bar{\mathbf{x}}}$ and mean covariance $\hat{\bar{\mathbf{P}}}$ can be calculated by equation B.8 and equation B.9 which will serve as input for the update phase.

$$\hat{\bar{\mathbf{x}}} = \sum_i w_i^m \boldsymbol{\mathcal{Y}}_i \tag{B.8}$$

$$\hat{\bar{\mathbf{P}}} = \sum_i w_i^c \left(\boldsymbol{\mathcal{Y}}_i - \hat{\bar{\mathbf{x}}}\right)\left(\boldsymbol{\mathcal{Y}}_i - \hat{\bar{\mathbf{x}}}\right)^T + \mathbf{Q} \tag{B.9}$$

The measurement input needs to be converted to the state vector format via $H()$:

$$\boldsymbol{\mathcal{Z}} = H(\boldsymbol{\mathcal{Y}}) \tag{B.10}$$

Next, the mean $\boldsymbol{\mu}_{\boldsymbol{\mathcal{Z}}}$ and the covariance matrix $\mathbf{P}_{\boldsymbol{\mathcal{Z}}}$ of the measurement data has to calculated as seen in equation B.11 and equation B.12:

$$\boldsymbol{\mu}_{\boldsymbol{\mathcal{Z}}} = \sum_i w_i^m \boldsymbol{\mathcal{Z}}_i \tag{B.11}$$

$$\mathbf{P}_{\boldsymbol{\mathcal{Z}}} = \sum_i w_i^c \left(\boldsymbol{\mathcal{Z}}_i - \hat{\bar{\mathbf{x}}}\right)\left(\boldsymbol{\mathcal{Z}}_i - \boldsymbol{\mu}_{\boldsymbol{\mathcal{Z}}}\right)^T + \mathbf{R} \tag{B.12}$$

The residual is obtained by:

$$\mathbf{y} = \boldsymbol{\mathcal{Z}} - \boldsymbol{\mu}_{\boldsymbol{\mathcal{Z}}} \tag{B.13}$$

The Kalman gain $\mathbf{K}$ is, similar to the KF case:

$$\mathbf{K} = \left( \sum_i w_i^c \left( \boldsymbol{\mathcal{Y}}_i - \hat{\bar{\mathbf{x}}} \right) \left( \boldsymbol{\mathcal{Y}}_i - \boldsymbol{\mu}_{\boldsymbol{\mathcal{Z}}} \right)^T \right) \mathbf{P}_{\boldsymbol{\mathcal{Z}}}^{-1} \tag{B.14}$$

Lastly, the Kalman gain is used to calculate the *posterior* state vector and covariance (equation B.15, equation B.16).

$$\hat{\mathbf{x}}_{k+1|k+1} = \hat{\bar{\mathbf{x}}}_{k+1|k+1} + \mathbf{K}\mathbf{y} \tag{B.15}$$

$$\hat{\mathbf{P}}_{k+1|k+1} = \hat{\bar{\mathbf{P}}} - \mathbf{K}\mathbf{P}_{\boldsymbol{\mathcal{Z}}}\mathbf{K}^T \tag{B.16}$$

## B.5 RTS smoothing implementation

The RTS smoother continues with the UKF data and works backward from the timestep $N-1$ to the first sample. This way 'future' data is incorporated in the calculation of state and covariance. The calculation of the prior sigma points $\boldsymbol{\mathcal{Y}}$ and the mean state vector and covariance is the same as equation B.7, equation B.8 and equation B.9. For the initial step, the smoothed RTS covariance is:

$$\hat{\mathbf{P}}_{UKF,k+2|k+2} = \hat{\mathbf{P}}_{N|N} = \hat{\mathbf{P}}_{k+2|k+2} \tag{B.17}$$

The RTS mean state vector and covariance:

$$\hat{\bar{\mathbf{x}}}_{\mathbf{RTS}} = \sum_i w_i^m \boldsymbol{\mathcal{Y}}_i \tag{B.18}$$

$$\hat{\bar{\mathbf{P}}}_{\mathbf{RTS}} = \sum_i w_i^c \left( \boldsymbol{\mathcal{Y}}_i - \hat{\bar{\mathbf{x}}} \right) \left( \boldsymbol{\mathcal{Y}}_i - \hat{\bar{\mathbf{x}}} \right)^T + \mathbf{Q} \tag{B.19}$$

The cross-variance of the mean state vector and posterior state vector ($\hat{\mathbf{x}}_{k+1|k+1}$) is:

$$\mathbf{P}_{RTS} = \sum_i w_i^c \left( \boldsymbol{\mathcal{Y}}_i - \hat{\bar{\mathbf{x}}}_{\mathbf{RTS}} \right) \left( \boldsymbol{\chi} - \hat{\mathbf{x}}_{k+1|k+1} \right)^T \tag{B.20}$$

Calculate the Kalman gain for this instance:

$$\mathbf{K} = \mathbf{P}_{RTS} \hat{\mathbf{P}}_{k+1|k+1}^{-1} \tag{B.21}$$

Use the future information and correct the posterior state vector and covariance:

$$\hat{\mathbf{x}}_{UKF,k+1|k+1} = \hat{\mathbf{x}}_{k+1|k+1} + \left( \mathbf{K} \left( \hat{\mathbf{x}}_{k+1|k+1} - \hat{\bar{\mathbf{x}}}_{\mathbf{RTS}} \right)^T \right)^T \tag{B.22}$$

$$\hat{\mathbf{P}}_{UKF,k+1|k+1} = \hat{\mathbf{P}}_{k+1|k+1} + \mathbf{K} \left( \hat{\mathbf{P}}_{UKF,k+2|k+2} - \hat{\bar{\mathbf{P}}}_{\mathbf{RTS}} \right) \mathbf{K}^T \tag{B.23}$$

## B.6 Measurements, additional information

In this section, a collection of premature, or earlier output with a different take or perspective are presented that could be of interest in a future project.

**Table B.1:** Example data to illustrate the explanation of the difference between pseudo interpolation and the currently used interpolation method.

| Timestamp | Range 1 | Range 2 | Range 3 | Range 4 |
|---|---|---|---|---|
| 1 | - | 1200 mm | - | - |
| 2 | 800 mm | 1200 mm | | |
| 3 | 800 mm | 1200 mm | 3300 mm | |
| 4 | 800 mm | 1200 mm | 3300 mm | 5600 mm |
| 5 | 800 mm | 1250 mm | 3300 mm | 5600 mm |
| 6 | 860 mm | 1250 mm | 3300 mm | 5600 mm |

## B.6.1 UWB datacollection types

There are 3 different ways to format and present UWB data. In this section, those types are explained.

### B.6.1.1 Pseudo interpolated

In the plots below the UWB data is preprocessed differently than in chapter 6. There, the UWB error data (also presented in violin plots) is interpolated in section B.6.1.2. As explained in section 6.2 UWB ranging is a consecutive activity. If the update rate is relatively low, then a certain amount of displacement of the TAG can happen between each consecutive ranging. Because the localization algorithms use all the ranges to calculate the location of a TAG of one update cycle that amount of displacement could contribute to a significant error.

Originally, the UWB ranging data for each ANC [4] was simply repeated in a next ranging. This is visualized with some example data in table B.1.

The errors related to this way of *pseudo interpolating* or *data padding* are visualized in figure B.2 and figure B.3.

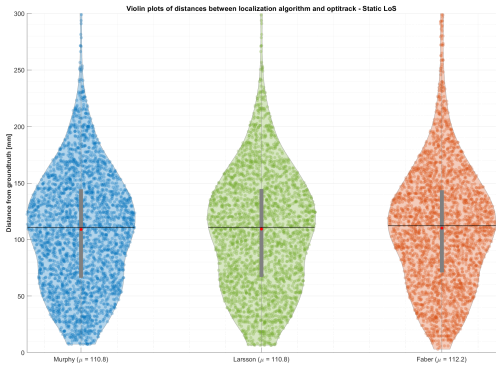


**Figure B.2:** A violin plot of UWB measurements (reference Optitrack). Average update rate 7.5 Hz. For each localization algorithm the mean ($\mu$) error is displaced at the rightside of the label.

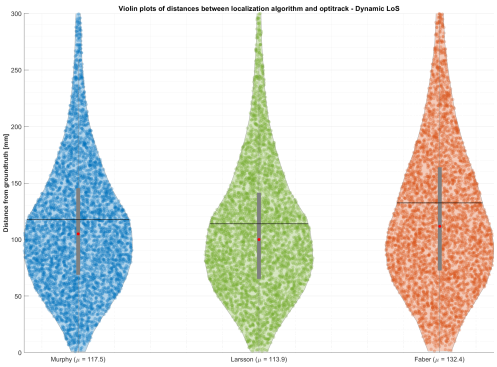


**Figure B.3:** A violin plot of UWB measurements (reference Optitrack). Average update rate 7.5 Hz. For each localization algorithm the mean ($\mu$) error is displaced at the rightside of the label.

### B.6.1.2 Interpolated

In figure 6.3 and figure 6.4 (in chapter 6) the UWB ranging data is used in linearly interpolated form.

[4] This means, for each TAG and ANC combination.

When the results in section B.6.1.1 are compared to figure 6.3 and figure 6.4 it can be observed that with regular interpolation the error is slightly lower.

### B.6.1.3 Localization timestamp

Another way of formatting the UWB data is by collecting the ranges of all TAG and ANC combinations and consider those to be collected at the first timestamp.

## B.7 Companies

This is an incomplete list of companies currently working on UWB technology [5]. In [36] different UWB products of three different companies (Bespoon, Ubisense and DecaWave) were compared. It is concluded that the DecaWave company produces the most accurate products.

**Table B.2:** List of companies which are working on UWB ranging technology with a selection of parameters. *reported accuracy.

| Name | Accuracy* | IMU | Price | Range | # Tags | samplefreq. | Protocol |
|---|---|---|---|---|---|---|---|
| Kinexon | decimeter | 9DoF | - | - | - | $60Hz$ | - |
| Pozyx | $10-30cm$ | - | - | - | 8 | $125Hz$ | TWR & *Time Difference of Arrival* (TDoA) |
| Infsoft | | - | - | - | - | - | - |
| DecaWave | | - | - | - | - | - | - |
| Eliko | $5-30cm$ | - | - | $70m$ | - | $40Hz$ | TDoA |
| Starix | NA | NA | NA | NA | - | - | - |
| Pulselink | | - | - | - | - | - | - |
| CUWB | centimeter | 9DoF | - | - | - | - | - |
| Sewio | decimeter | - | - | - | $\infty$ | - | - |
| Ubisense | - | no | - | - | - | *variable* | TDoA & *Angle-of-Arrival* (AoA) |
| Bespoon | $\leq 10cm$ | no | - | $600m$ | - | $< 200Hz$ | TWR |
| UwinLoc | - | no | - | - | - | $\leq 1$ Hz | - |

## B.8 Wheelchair sport parameters

This section covers some of the wheelchair sport parameters of importance to this project.

As seen in figure B.4 the court size is 24 m by 11 m. The minimum number of players is 2, the maximum number of players is 4. Figure B.5 illustrates the wheelchair rugby court size of 28 m by 15 m. The maximum number of players on the court is 8. Every team has a maximum number of players of 12.

### B.8.1 Anchor placement dimensions

The maximum wheelchair court size is 28 m by 15 (rugby). In tennis a court size of 24 m by 11 m is used. Because the ANCs can not be on the perimeter or in the field, and some margin is needed for localizing players close to the perimeter of the court an additional distance of 2 m is added to each side of the court making the dimensions: 28 m **by** 15 m.

[5] source1,source2

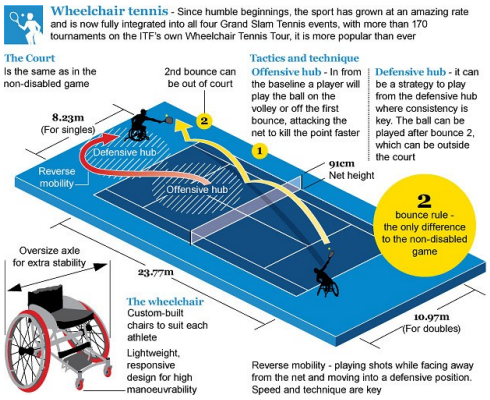


**Figure B.4:** Size of wheelchair tennis court. Source: Telegraph.co.uk .

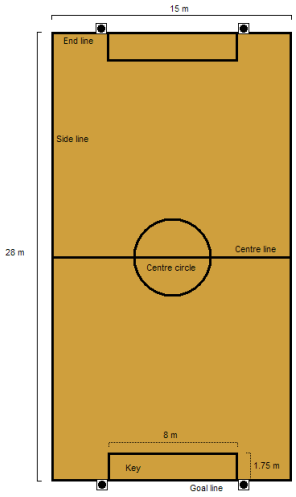


**Figure B.5:** Size of wheelchair tennis court Source Wikipedia.